

# Dynamic magnetic susceptibility and electrical detection of ferromagnetic resonance

Yin Zhang,<sup>1,2</sup> X. S. Wang,<sup>1,2</sup> H. Y. Yuan,<sup>1,2</sup> S. S. Kang,<sup>3</sup> H. W. Zhang,<sup>4</sup> and X. R. Wang<sup>1,2,\*</sup>

<sup>1</sup>*Physics Department, The Hong Kong University of Science and Technology, Clear Water Bay, Kowloon, Hong Kong*

<sup>2</sup>*HKUST Shenzhen Research Institute, Shenzhen 518057, China*

<sup>3</sup>*School of Physics, National Key Laboratory of Crystal Materials, Shandong University, Jinan, Shandong 250100, China*

<sup>4</sup>*School of Microelectronics and Solid-State Electronics,*

*University of Electronic Science and Technology of China, Chengdu, Sichuan 610054, China*

(Dated: December 8, 2015)

The dynamic magnetic susceptibility of magnetic materials near ferromagnetic resonance (FMR) is very important in interpreting dc-voltage obtained in an electrical detection of FMR. Based on the causality principle and the assumption that the usual microwave absorption lineshape around FMR is Lorentzian, general forms of dynamic magnetic susceptibility of an arbitrary sample and the corresponding dc-voltage lineshapes of the electrical detection of FMR are obtained. Our main findings are: 1) The dynamic magnetic susceptibility is not a Polder tensor for a material with an arbitrary magnetic anisotropy. Two off-diagonal matrix elements of the tensor near FMR are not in general opposite to each other. However, the linear response coefficient of the magnetization to the total radio frequency (rf) field (sum of the applied external rf field and the internal rf field due to the precessing magnetization, a quantity cannot be measured directly) is a Polder tensor. This may explain why two off-diagonal susceptibility matrix elements are always assumed to be opposite to each other in analyses. 2) The frequency dependence of dynamic magnetic susceptibility near FMR is fully characterized by six *real* numbers while its field dependence is fully characterized by seven *real* numbers. 3) A recipe of how to determine these numbers by standard microwave absorption measurements for a sample with an arbitrary magnetic anisotropy is proposed. Our results allow one to unambiguously separate the contribution of the anisotropic magnetoresistance to dc-voltage signals from that of the anomalous Hall effect. With these results, one can reliably extract the information of spin pumping and the inverse spin Hall effect, and determine the spin-Hall angle. 4) The field-dependence of the susceptibility matrix elements at a fixed microwave frequency may have several peaks when the effective magnetic field is not a monotonic function of the applied magnetic field. In contrast, the frequency-dependence of the susceptibility matrix elements at a fixed applied magnetic field has only one FMR peak. Furthermore, in the case that resonance frequency is not sensitive to the externally applied static magnetic field, the field dependence of matrix elements of the dynamic magnetic susceptibility, as well as dc-voltage, may have another non-resonance broad peak. Thus, one should be careful in interpreting observed peaks.

## I. INTRODUCTION

Ferromagnetic resonance (FMR) is an important phenomenon which can be used to probe magnetic properties of ferromagnetic materials besides many other applications<sup>1–6</sup>. Microwave absorption is usually measured in traditional FMR experiments, and the absorption lineshape around FMR is a Lorentzian function of microwave frequency for a fixed static magnetic field. The peak position and peak width can be used to determine magnetic anisotropy and the Gilbert damping coefficient<sup>7,8</sup>. In recent years, the electrical detection of FMR, in which a dc-voltage is measured on a sample around FMR, becomes very popular due to the high accuracy of dc-voltage measurements and only microns sample size needed<sup>9–23</sup>. This technique has been used by many groups<sup>11–17</sup> in recent years to extract spin pumping and the spin Hall angle that measures the strength of both the spin Hall effect (SHE) and the inverse spin Hall effect (ISHE). However, the experimentally extracted material parameters show a large discrepancy for the same materials with similar experimental setup. For example, the spin Hall angle of Pt obtained

by different groups differs from each other by two orders of magnitude<sup>13–15</sup> due to different interpretations of the dc-voltage signal.

The dc-voltage in an electrical detection of FMR can come from two sources. One is the generalized Ohm's law in which the well-known anisotropic magnetoresistance (AMR) and anomalous Hall effect (AHE) couple the magnetization motion with the electric current (see the discussion below)<sup>9,10,19</sup>. This coupling between the magnetization and microwave-induced electric current results in the so-called spin rectification effect<sup>19</sup> that gives rise to a detectable dc-voltage inside a magnetic layer or multilayer at FMR. The other dc-voltage source is the ISHE: a spin current converts into a transverse charge current via ISHE inside a multilayer, and the charge current, in turn, gives rise to a dc-voltage. In the popular spin-Hall-angle experiments<sup>11–13,16,17</sup>, the spin current comes from spin pumping by magnetization precession at FMR<sup>24,25</sup>. To use the electrical detection of FMR as a probe of material properties, one needs to separate different dc-voltage sources. A common way is the symmetry analysis of dc-voltage lineshapes. The ISHE contribution to dc-voltage is normally assumed to have a symmetric

lineshape<sup>11–17</sup>, resembling microwave absorption curves. The AMR contribution to dc-voltage can be symmetric<sup>17</sup>, antisymmetric<sup>13</sup> or asymmetric<sup>15,16</sup> although resistance normally links to energy dissipation. On the other hand, the AHE contribution can be antisymmetric<sup>11,17</sup> or vanishing small<sup>13,15,16</sup> because the Hall effect does not necessarily involve energy dissipation, depending on material properties and experimental setup. So far, most analyses<sup>11–13,15,16,19</sup> assume that the static response of magnetization is always along the external magnetic field so that the microwave-induced magnetization precession is around the external static magnetic field. Furthermore, the two off-diagonal matrix elements of the dynamic magnetic susceptibility are assumed to be opposite to each other. However, both assumptions are questionable for layer/multilayer samples. Interfacial spin-orbit interactions and/or other interactions may modify the magnetic anisotropy of a film<sup>26–28</sup>. As we shall see below, the dynamic magnetic susceptibility of a sample with non-zero magnetic anisotropy is not a Polder tensor in general. For a given experimental setup, the dc-voltage due to AMR and AHE is very sensitive to the dynamic magnetic susceptibility since the spin rectification effect comes from the phase lag of radio frequency (rf) magnetization precession and rf current. Thus, the dynamic magnetic susceptibility at FMR is a central quantity.

In this work, we obtain general expressions of the dynamic magnetic susceptibility matrix of an arbitrary magnetic material near FMR based on the causality principle and the fact that microwave absorption at FMR is a Lorentzian in microwave frequency at a fixed static magnetic field. The dynamic magnetic susceptibility is not a Polder tensor in general. It becomes a Polder tensor when the sample is isotropic or uniaxial with the static magnetic field along its easy-axis. The matrix is fully characterized by a few constants that can be determined by traditional microwave absorption experiments. Interestingly, the linear response coefficient of the magnetization to the total rf field, the sum of the applied external rf field and the internal rf field due to the magnetization precession, is a Polder tensor. However, this coefficient is not the dynamic magnetic susceptibility, and cannot be measured directly. Furthermore, under a fixed rf, the susceptibility matrix elements may have multiple peaks in the field at a fixed microwave frequency in contrast to a single peak in frequency at a fixed field. The multiple field peaks come from the non-monotonic behavior of the total effective magnetic field to the externally applied static magnetic field. With the knowledge on the dynamic magnetic susceptibility matrix, it is possible to separate the contributions of the AMR to the dc-voltage from that of the AHE. We also show that another broad peak may appear in the susceptibility matrix elements if the resonance frequency is not very sensitive to the externally applied magnetic field. In turn, a broad peak might also appear in the field-dependence of the microwave absorption curves as well as the dc-voltage lineshape. This peak is not from the resonance, and its shape is not

Lorentzian. The paper is organized as follows. In Sec. II we first reformulate the generalized Ohm's law for a magnetic metal, and explain how a dc-voltage can come out of the spin rectification at FMR. Then we derive the expression of the dynamic magnetic susceptibility matrix both as a function of microwave frequency or as a function of static magnetic field. The experimental method of determining the matrix is then given. With the dynamic magnetic susceptibility matrix, we analyse the dc-voltage from AMR and AHE. Section III uses several examples to verify the general form of the dynamic magnetic susceptibility matrix obtained in Sec. II. We show how multiple FMR peaks in field at a fixed frequency can come from the non-monotonic behavior of the effective field in applied field, and how a non-resonance peak can arise when the resonance frequency (or effective field) is not sensitive to the externally applied static magnetic field. The conclusion is given in Sec. IV, followed by acknowledgment.

## II. THEORETICAL ANALYSIS

### A. The generalized Ohm's law and spin rectification

The electrical detection of FMR is based on the generalized Ohm's law in a polycrystalline ferromagnetic metal<sup>9,10,19</sup>

$$\mathbf{E} = \rho_{\perp} \mathbf{J} + \frac{\Delta\rho}{M^2} (\mathbf{J} \cdot \mathbf{M}) \mathbf{M} - R_0 \mathbf{J} \times \mathbf{H} - R_1 \mathbf{J} \times \mathbf{M}, \quad (1)$$

where  $M$  is the magnitude of magnetization  $\mathbf{M}$ ,  $\mathbf{H}$  and  $\mathbf{J}$  are respectively the magnetic field and the electric current density.  $\rho_{\perp}$  is the longitudinal resistivity when  $\mathbf{M}$  and  $\mathbf{J}$  are perpendicular with each other.  $\Delta\rho = \rho_{\parallel} - \rho_{\perp}$  is the difference between  $\rho_{\perp}$  and the longitudinal resistivity  $\rho_{\parallel}$  when  $\mathbf{M}$  is parallel to  $\mathbf{J}$ , and the  $\Delta\rho$ -term is called AMR.  $R_0$  and  $R_1$  describe respectively the ordinary and anomalous Hall effects.

Eq. (1) is in fact the most general linear response of electric field of a polycrystalline magnet to an applied electric current density. It could be understood by the following reasoning. For simplicity, let us assume that there is no external field ( $\mathbf{H} = 0$ ). For the linear response of the electric field  $\mathbf{E}$  to an electric current density  $\mathbf{J}$ , the most general expression of  $\mathbf{E}$  must be  $\mathbf{E} = \overleftrightarrow{\rho}(\mathbf{M})\mathbf{J}$ , where  $\overleftrightarrow{\rho}(\mathbf{M})$  is a rank-2 Cartesian tensor that depends on  $\mathbf{M}$  since  $\mathbf{M}$  is the only available vector. It is well-known that a Cartesian tensor of rank 2 can be decomposed into the direct sum of a scalar of function of  $M$ , a vector that is a function of  $M$  multiplying  $\mathbf{M}$ , and a traceless symmetric tensor of a function of  $M$  multiplying  $\mathbf{M}\mathbf{M} - M^2/3$ . Thus the most general expression of  $\mathbf{E}$  is  $\mathbf{E} = (\rho_{\perp} + \Delta\rho/3)\mathbf{J} + R_1\mathbf{M} \times \mathbf{J} + (\Delta\rho/M^2)(\mathbf{M}\mathbf{M} - M^2/3) \cdot \mathbf{J}$ . This is exactly Eq. (1), and no new physics is obtained from this reasoning. However, things are very different if we carry out the similar analysis for a poly-

crystalline magnetic film lying in the  $xy$ -plane. Although the polycrystalline sample is isotropic in the film plane,  $\hat{z}$  is an available vector and  $\vec{\rho}(\mathbf{M}, \hat{z})$  should be a function of both  $\mathbf{M}$  and  $\hat{z}$ . Since three vectors ( $\mathbf{M}$ ,  $\hat{z}$ , and  $\mathbf{M} \times \hat{z}$ ) and three traceless symmetric tensors ( $\mathbf{M}\mathbf{M} - M^2/3$ ,  $\mathbf{M}\hat{z} + \hat{z}\mathbf{M} - 2M_z/3$ , and  $\hat{z}\hat{z} - 1/3$ ), can be constructed out of  $\mathbf{M}$  and  $\hat{z}$  we have, with similar reasoning as we used early for polycrystalline magnetic bulk,  $\mathbf{E} = (\rho_{\perp} + \Delta\rho/3 + \rho_2/3)\mathbf{J} + (R_1\mathbf{M} + \rho_1\hat{z} + R_2'\mathbf{M} \times \hat{z}) \times \mathbf{J} + [(\Delta\rho/M^2)(\mathbf{M}\mathbf{M} - M^2/3) + R_3'(\mathbf{M}\hat{z} + \hat{z}\mathbf{M} - 2M_z/3)] \cdot \mathbf{J} + \rho_2(\hat{z}\hat{z} - 1/3) \cdot \mathbf{J} = \rho_{\perp}\mathbf{J} - R_1\mathbf{J} \times \mathbf{M} + (\Delta\rho/M^2)(\mathbf{M} \cdot \mathbf{J})\mathbf{M} - \rho_1\mathbf{J} \times \hat{z} + R_2(\hat{z} \cdot \mathbf{J})\mathbf{M} + R_3(\mathbf{M} \cdot \mathbf{J})\hat{z} - R_4M_z\mathbf{J} + \rho_2(\hat{z} \cdot \mathbf{J})\hat{z}$ , where  $R_2 \equiv R_2' + R_3'$ ,  $R_3 \equiv R_3' - R_2'$  and  $R_4 \equiv (2/3)R_2'$ . The  $\rho_1$ -term may be interpreted as the spin-Hall term if the sign of  $\rho_1$  for spin-up electrons is opposite to that for spin-down electrons. It is known that spin-orbit interactions can lead to a term like this. Obviously,  $\rho_2$  contributes to the longitudinal resistivity along  $z$ -direction. Interestingly, three new terms are obtained: 1) A current perpendicular to the film induces an electric field in  $\mathbf{M}$  direction (the  $R_2$ -term). 2) A current along  $\mathbf{M}$  direction generates an electric field in  $\hat{z}$  direction ( $R_3$ -term). 3) The  $R_4$ -term says that resistance of the film depends on  $M_z$  linearly. Of course, the coefficients of these terms depend, in principle, on  $M$ . It should be pointed out that the interfacial effects are very common in physics.<sup>29</sup> Generally speaking, all new terms should exist in polycrystalline magnetic films. Of course, their values depend on microscopic interactions that lead to these terms. However, these terms are not the subjects of this study although they deserve a careful and in-depth investigation<sup>30</sup>. We shall only concentrate on AMR and AHE in Eq. (1).

Let us come back to dc-voltage in the electrical detection of FMR in which electric current density  $\mathbf{J} = \text{Re}(\mathbf{j}e^{-i(\omega t + \phi_1)})$  comes from the rf electric field only, where  $\omega$  and  $\phi_1$  are respectively the microwave frequency and the phase lag of the electric current with the electric field.  $\phi_1$  is a material parameter that depends on the complex electric conductivity. The rf magnetic field  $\text{Re}(\mathbf{h}e^{-i(\omega t + \phi_2)})$  exerts a torque on  $\mathbf{M}$ , causing magnetization precession around a static magnetization  $\mathbf{M}_0$  that is determined by the external static magnetic field and magnetic anisotropy.  $\phi_2$  is the phase difference between the rf electric field and  $\mathbf{h}$  inside the sample, and its value depends on the particular experimental setup and the material parameters like dielectric constant. For example,  $\phi_2 = \phi_1$  in those experiments<sup>13,14</sup> in which the rf magnetic field is generated by the rf electric current. However, in other experiments<sup>11,15,17</sup> with microwave cavities,  $\phi_2$  differs from  $\phi_1$ . Since both  $\phi_1$  and  $\phi_2$  are material parameters and depend on experimental setup, we will treat them as input parameters.

The magnetization  $\mathbf{M} = \mathbf{M}_0 + \text{Re}(\mathbf{m}e^{-i(\omega t + \phi_2)})$  contains a small component precessing at frequency  $\omega$ . Phase  $\phi_2$  is added in our definition of  $\mathbf{m}$  for convenience. Using  $\langle \dots \rangle$  to denote the time average, the dc-voltage is

given by

$$U = \langle \mathbf{E} \rangle \cdot \mathbf{l}, \quad (2)$$

where  $\mathbf{l}$  is the displacement vector between two electrode contact points on the sample film. Since  $\langle \text{Re}(\mathbf{m}e^{-i(\omega t + \phi_2)}) \rangle = 0$  and  $\langle \mathbf{J} \rangle = 0$ , the dc-voltage comes from the terms in Eq. (1) that contain  $\langle \text{Re}(\mathbf{j}e^{-i(\omega t + \phi_1)}) \cdot \text{Re}(\mathbf{m}e^{-i(\omega t + \phi_2)}) \rangle$  and  $\langle \text{Re}(\mathbf{j}e^{-i(\omega t + \phi_1)}) \times \text{Re}(\mathbf{m}e^{-i(\omega t + \phi_2)}) \rangle$ , resulting in the spin rectification.  $\langle \mathbf{E} \rangle$  reads as

$$\begin{aligned} \langle \mathbf{E} \rangle = & \frac{\Delta\rho}{2M^2} \text{Re}\{(\mathbf{j}^* \cdot \mathbf{m}e^{i(\phi_1 - \phi_2)})\mathbf{M}_0 + (\mathbf{j}^* \cdot \mathbf{M}_0)\mathbf{m}e^{i(\phi_1 - \phi_2)}\} \\ & - \frac{R_0}{2} \text{Re}(\mathbf{j}^* \times \mathbf{h}e^{i(\phi_1 - \phi_2)}) - \frac{R_1}{2} \text{Re}(\mathbf{j}^* \times \mathbf{m}e^{i(\phi_1 - \phi_2)}), \end{aligned} \quad (3)$$

where the first and the second terms on the right-hand side (RHS) come from the AMR and the last two terms arise respectively from the ordinary and anomalous Hall effects. It is convenient to define a Cartesian coordinate system  $(x, y, z)$ , where  $z$ -axis is along  $\mathbf{M}_0$ . The ordinary Hall effect can be neglected since it is much smaller than the AMR and AHE in a ferromagnetic metal<sup>9,31</sup>. By substituting Eq. (3) into Eq. (2), the AMR and AHE contributions to dc-voltage are

$$U_{\text{AMR}} = \frac{\Delta\rho}{2M} \text{Re}\{[(\mathbf{j}^* \cdot \mathbf{m})l_z + j_z^*(\mathbf{m} \cdot \mathbf{l})]e^{i(\phi_1 - \phi_2)}\}, \quad (4)$$

$$U_{\text{AHE}} = -\frac{R_1}{2} \text{Re}[(\mathbf{j}^* \times \mathbf{m}) \cdot \mathbf{l}e^{i(\phi_1 - \phi_2)}]. \quad (5)$$

Once the phase difference  $\phi_1 - \phi_2$  between  $\mathbf{j}$  and  $\mathbf{h}$  is given by experimental setup and material parameters, the dc-voltage depends on how  $\mathbf{m}$  responds to  $\mathbf{h}$ , or the dynamic magnetic susceptibility near FMR.

## B. Universal form of dynamic magnetic susceptibility matrix

It is important to obtain the dynamic magnetic susceptibility  $\vec{\chi}$  because the dc-voltage in electrical detection of FMR depends on  $\vec{\chi}$ . Under a microwave radiation, magnetization precession is governed by the Landau-Lifshitz-Gilbert (LLG) equation<sup>32</sup>:

$$\frac{\partial \mathbf{M}}{\partial t} = -\gamma \mathbf{M} \times \mathbf{H}_{\text{eff}} + \frac{\alpha}{M} \mathbf{M} \times \frac{\partial \mathbf{M}}{\partial t}, \quad (6)$$

where  $\mathbf{H}_{\text{eff}}$  is the effective field which includes the applied static magnetic field  $\mathbf{H}$ , rf magnetic field  $\text{Re}(\mathbf{h}e^{-i(\omega t + \phi_2)})$  and anisotropy field.  $\alpha$  is the Gilbert damping coefficient. This is a nonlinear equation that has many interesting physics, including spin wave emission by magnetic domain wall motion<sup>33</sup>, and can only be solved for a few special issues<sup>34</sup>. However, if the amplitude of  $\mathbf{h}$  is small enough, the linear response of  $\mathbf{m}$  to  $\mathbf{h}$  can be obtained

from the linearized LLG Eq. and takes the following form,

$$\begin{pmatrix} m_x \\ m_y \\ m_z \end{pmatrix} = \begin{pmatrix} \chi_{xx} & \chi_{xy} & 0 \\ \chi_{yx} & \chi_{yy} & 0 \\ 0 & 0 & 0 \end{pmatrix} \begin{pmatrix} h_x \\ h_y \\ h_z \end{pmatrix}. \quad (7)$$

The structure of Eq. (7) comes from the facts that  $\mathbf{m}$  is perpendicular to  $\mathbf{M}_0$  ( $m_z = 0$ ) and  $h_z$  does not exert any torque on  $\mathbf{M}$  so that  $\mathbf{m}$  does not depend on  $h_z$ .

The energy change rate of the system can be written as

$$\frac{d\varepsilon}{dt} = \nabla_{\mathbf{M}}\varepsilon \cdot \frac{\partial \mathbf{M}}{\partial t} - \mu_0 \mathbf{M} \cdot \frac{\partial \mathbf{H}_e}{\partial t} \quad (8)$$

where  $\varepsilon$  is the energy density of the system, and  $\mathbf{H}_e \equiv \mathbf{H} + \text{Re}(\mathbf{h}e^{-i(\omega t + \phi_2)})$  is the total applied field. Notice Eq. (6) can also be casted as

$$\frac{\partial \mathbf{M}}{\partial t} = -\frac{\gamma}{1 + \alpha^2} \mathbf{M} \times \mathbf{H}_{\text{eff}} - \frac{\alpha\gamma}{(1 + \alpha^2)M} \mathbf{M} \times (\mathbf{M} \times \mathbf{H}_{\text{eff}}). \quad (9)$$

Substituting  $\nabla_{\mathbf{M}}\varepsilon = -\mu_0 \mathbf{H}_{\text{eff}}$  and Eq. (9) into Eq. (8), one obtains

$$\frac{d\varepsilon}{dt} = -\frac{\alpha\gamma\mu_0}{(1 + \alpha^2)M} |\mathbf{M} \times \mathbf{H}_{\text{eff}}|^2 - \mu_0 \mathbf{M} \cdot \dot{\mathbf{H}}_e. \quad (10)$$

The first term on the RHS of Eq. (10) is the energy dissipation due to the motion of magnetization while the second term describes the energy release/absorption rate from the microwave. Since the total energy of a system cannot increase or decrease indefinitely, the time average of the energy change rate should be zero,  $\langle \dot{\varepsilon} \rangle = 0$  so that the average microwave absorption (by the sample) rate  $I$  should be equal to energy dissipation rate<sup>35</sup>.  $I$  reads

$$I = -\mu_0 \langle \mathbf{M} \cdot \dot{\mathbf{H}}_e \rangle = -\frac{\mu_0\omega}{2} \text{Im}(\mathbf{m}^* \cdot \mathbf{h}), \quad (11)$$

and by substituting Eq. (7) into Eq. (11),  $I$ , in terms of  $\overleftrightarrow{\chi}$ , becomes

$$I = \frac{\mu_0\omega}{2} [h_x^* h_x \chi''_{xx} + \text{Re}(h_x^* h_y)(\chi''_{xy} + \chi''_{yx}) + \text{Im}(h_x^* h_y)(\chi'_{xy} - \chi'_{yx}) + h_y^* h_y \chi''_{yy}], \quad (12)$$

where  $\chi_{jk} = \chi'_{jk} + i\chi''_{jk}$  ( $j, k = x, y$ ). It is known that microwave absorption intensity as a function of microwave frequency at a fixed static magnetic field is Lorentzian. We shall use this property and the causality principle (events come after causes)<sup>36</sup> to find both  $\overleftrightarrow{\chi}(\omega)$  and  $\overleftrightarrow{\chi}(H)$  below.

### 1. Frequency dependence of $\overleftrightarrow{\chi}$

In the case that the microwave frequency  $\omega$  is swept at a fixed static magnetic field  $H$ , each element of  $\overleftrightarrow{\chi}(\omega)$  should be analytic in the up-half complex  $\omega$ -plane due

to the causality principle (events come after causes)<sup>36</sup>. The consequence is that its real and imaginary parts are related to each other by the Kramers-Kronig relations. In the resonance region and in the absence of high-order contribution, the energy absorption intensity is a Lorentzian function  $L(\omega, \omega_0, \Gamma)$ ,

$$L(\omega, \omega_0, \Gamma) = \frac{1}{\pi} \frac{\frac{\Gamma}{2}}{(\omega - \omega_0)^2 + (\frac{\Gamma}{2})^2}. \quad (13)$$

The counterpart of  $L(\omega, \omega_0, \Gamma)$  in the Kramers-Kronig relations is the function  $D(\omega, \omega_0, \Gamma)$ ,

$$D(\omega, \omega_0, \Gamma) = \frac{1}{\pi} \frac{\omega - \omega_0}{(\omega - \omega_0)^2 + (\frac{\Gamma}{2})^2}, \quad (14)$$

where  $\omega_0$  denotes the resonance frequency and  $\Gamma$  is the linewidth which is a positive number.  $D$  can be both positive and negative, and extends further in comparison to  $L(\omega, \omega_0, \Gamma)$ . Since the energy absorption lineshape should be Lorentzian for an arbitrary  $\mathbf{h}$ , each term on the RHS of Eq. (12) should have the form of Eq. (13) with the same resonance frequency  $\omega_0$  and linewidth  $\Gamma$ :

$$\begin{aligned} \chi''_{xx}(\omega) &= C_1 \left(\frac{\pi\Gamma}{2}\right) L(\omega, \omega_0, \Gamma), \\ \chi''_{xy}(\omega) + \chi''_{yx}(\omega) &= 2C_2 \left(\frac{\pi\Gamma}{2}\right) L(\omega, \omega_0, \Gamma), \\ \chi'_{xy}(\omega) - \chi'_{yx}(\omega) &= 2C_3 \left(\frac{\pi\Gamma}{2}\right) L(\omega, \omega_0, \Gamma), \\ \chi''_{yy}(\omega) &= C_4 \left(\frac{\pi\Gamma}{2}\right) L(\omega, \omega_0, \Gamma), \end{aligned} \quad (15)$$

where the four *real* numbers  $C_1 \sim C_4$  are determined by the material parameters and experimental setup. A factor of  $\pi\Gamma/2$  is introduced in order to make  $C_i$  ( $i = 1, 2, 3, 4$ ) dimensionless. By using the Kramers-Kronig relations, one can write

$$\begin{aligned} \chi'_{xx}(\omega) &= -C_1 \left(\frac{\pi\Gamma}{2}\right) D(\omega, \omega_0, \Gamma), \\ \chi'_{xy}(\omega) + \chi'_{yx}(\omega) &= -2C_2 \left(\frac{\pi\Gamma}{2}\right) D(\omega, \omega_0, \Gamma), \\ \chi''_{xy}(\omega) - \chi''_{yx}(\omega) &= 2C_3 \left(\frac{\pi\Gamma}{2}\right) D(\omega, \omega_0, \Gamma), \\ \chi'_{yy}(\omega) &= -C_4 \left(\frac{\pi\Gamma}{2}\right) D(\omega, \omega_0, \Gamma). \end{aligned} \quad (16)$$

From Eqs. (15) and (16),  $\overleftrightarrow{\chi}(\omega)$  should have the general form of

$$\overleftrightarrow{\chi}(\omega) = \frac{\pi\Gamma}{2} [L(\omega, \omega_0, \Gamma) + iD(\omega, \omega_0, \Gamma)] \overleftrightarrow{C}, \quad (17)$$

where

$$\overleftrightarrow{C} = \begin{pmatrix} iC_1 & C_3 + iC_2 & 0 \\ -C_3 + iC_2 & iC_4 & 0 \\ 0 & 0 & 0 \end{pmatrix}. \quad (18)$$

Thus  $\overleftrightarrow{\chi}(\omega)$  of an arbitrary magnet is completely determined by six numbers  $\omega_0$ ,  $\Gamma$ ,  $C_1$ ,  $C_2$ ,  $C_3$  and  $C_4$ . Interestingly, the two off-diagonal matrix elements of  $\overleftrightarrow{\chi}(\omega)$  are not opposite to each other in general, because  $C_2$  is zero only when the material has certain special symmetry or for a special coordinate (see discussion in Section II.C).

In terms of phase  $\psi \equiv \cot^{-1}[-D/L] = \cot^{-1}[(\omega_0 - \omega)/\Gamma]$ ,  $\mathbf{m}$  relates to  $\mathbf{h}$  as

$$\mathbf{m} = \begin{pmatrix} |\chi_{xx}| & |\chi_{xy}|e^{-i\cot^{-1}\frac{C_2}{C_3}} & 0 \\ |\chi_{yx}|e^{i\cot^{-1}\frac{C_2}{C_3}} & |\chi_{yy}| & 0 \\ 0 & 0 & 0 \end{pmatrix} \mathbf{h}e^{i\psi}. \quad (19)$$

When microwave frequency  $\omega$  is swept through FMR region at a fixed static magnetic field, the phase  $\psi$  changes from  $0^\circ$  to  $180^\circ$  and is  $90^\circ$  at FMR. This property of  $\psi$  is universal for an arbitrary system.

## 2. Field dependence of $\overleftrightarrow{\chi}$

In most experiments, the microwave frequency was fixed and the applied static magnetic field was swept. Thus, it is also useful to obtain the field dependence of  $\overleftrightarrow{\chi}$ . One cannot directly apply the causality principle here, and we shall use Eq. (17). Notice that each of  $\omega_0$ ,  $\Gamma$  and  $\overleftrightarrow{C}$  is a function of  $H$ ,  $\overleftrightarrow{\chi}$  can be expressed as

$$\overleftrightarrow{\chi}(H) = \frac{\pi\Gamma(H)}{2}[L(\omega, \omega_0(H), \Gamma(H)) + iD(\omega, \omega_0(H), \Gamma(H))]\overleftrightarrow{C}(H). \quad (20)$$

Unlike the frequency sweeping case where  $\mathbf{M}_0$  is always in the same direction,  $\mathbf{M}_0$  changes its direction during the field sweeping process (in which the direction of  $\mathbf{H}$  does not change). However, one expects that  $\omega_0$ ,  $\Gamma$  and  $\overleftrightarrow{C}$  do not change much if the FMR peak width is narrow. Thus one can replace  $\mathbf{M}_0$ ,  $\Gamma$  and  $\overleftrightarrow{C}$  by their values at the resonance field  $H_0$  where  $\omega_0(H_0) = \omega$ ,

$$\begin{aligned} \mathbf{M}_0(H) &\approx \mathbf{M}_0(H_0), \\ \Gamma(H) &\approx \Gamma(H_0), \\ \overleftrightarrow{C}(H) &\approx \overleftrightarrow{C}(H_0). \end{aligned} \quad (21)$$

Similarly, one can expand  $\omega_0(H)$  around  $H_0$  to the linear order in  $H - H_0$ ,

$$\omega_0(H) \approx \omega + \beta(H - H_0). \quad (22)$$

Substituting Eqs. (21) and (22) into Eq. (20), one has

$$\overleftrightarrow{\chi}(H) = \frac{\pi\Gamma_1}{2}[L(H, H_0, \Gamma_1) + i\frac{-\beta}{|\beta|}D(H, H_0, \Gamma_1)]\overleftrightarrow{C}(H_0), \quad (23)$$

where  $\Gamma_1$  is the linewidth of the field:

$$\Gamma_1 = \frac{\Gamma(H_0)}{|\beta|}. \quad (24)$$

It is not surprising to see that  $\Gamma_1$  is large if  $\omega_0(H)$  does not change much around  $H_0$  (small  $\beta$ ) while it is smaller for a larger  $\beta$ . Similar to the frequency dependence of  $\overleftrightarrow{\chi}$ , the field dependence of  $\overleftrightarrow{\chi}$  around a FMR is fully determined by six numbers,  $H_0$ ,  $\Gamma_1$ ,  $C_1$ ,  $C_2$ ,  $C_3$  and  $C_4$ . However, the sign in front of  $D$  function in Eq. (23) is decided by the sign of  $\beta$  (“+” when  $\omega_0$  decreases with  $H$  and “-” otherwise). In terms of phase  $\psi \equiv \cot^{-1}[(\beta/|\beta|)D/L] = \cot^{-1}[(\beta/|\beta|)(H - H_0)/\Gamma_1]$ , the  $\beta$ -sign decides whether  $\psi$  changes from  $180^\circ$  to  $0^\circ$  or from  $0^\circ$  to  $180^\circ$  when the field is swept up through the resonance region. The sign also relates to the sign of dc voltage as well as whether the observed signal, like  $dI/dH$  in traditional microwave absorption measurement, increases or decreases with  $H$ . This is in contrast to the frequency dependence of  $\overleftrightarrow{\chi}$  as shown in Eq. (17), where the sign before  $D$  function is always positive so that phase  $\psi$  always increases from  $0^\circ$  far under the resonance frequency ( $\omega \ll \omega_0$ ) to  $180^\circ$  far above the resonance frequency ( $\omega \gg \omega_0$ ). Obviously,  $\overleftrightarrow{\chi}(H)$  is not a Polder tensor in general.  $\overleftrightarrow{\chi}(H)$  may deviate from Eq. (23) when approximation of Eq. (21) is not good. As a result, a non-resonance broad peak and symmetry changes in elements of  $\overleftrightarrow{\chi}(H)$  can occur. Explicit examples will be discussed in Section III.B.

## C. The Polder or Non-Polder tensors

In order to understand why the Polder tensor was always used in experimental analyses, we want to see which linear response coefficient is a Polder tensor. Assume  $\mathbf{H}_K(\mathbf{M})$  is the anisotropy field, then, to the first order in  $\mathbf{m}$ , the effective field is

$$\begin{aligned} \mathbf{H}_{\text{eff}} &= \mathbf{H} + \mathbf{H}_K(\mathbf{M}_0) + \\ \nabla_{\mathbf{M}}\mathbf{H}_K|_{\mathbf{M}_0} \cdot \mathbf{m}e^{-i(\omega t + \phi_2)} &+ \mathbf{h}e^{-i(\omega t + \phi_2)}. \end{aligned} \quad (25)$$

Substituting Eq. (25) and  $\mathbf{M} = \mathbf{M}_0 + \mathbf{m}e^{-i(\omega t + \phi_2)}$  into Eq. (6), one has, up to the linear term in  $\mathbf{m}$ ,

$$-i\omega\mathbf{m} = -\gamma\mathbf{m} \times \mathbf{H}_{\text{dc}} - \gamma\mathbf{M}_0 \times \mathbf{h}_{\text{ac}} - i\omega\frac{\alpha}{M}\mathbf{M}_0 \times \mathbf{m}, \quad (26)$$

where  $\mathbf{H}_{\text{dc}}$  is the effective dc-field

$$\mathbf{H}_{\text{dc}} = \mathbf{H} + \mathbf{H}_K(\mathbf{M}_0) \quad (27)$$

and  $\mathbf{h}_{\text{ac}}$  is the effective ac-field that is the sum of applied rf field  $\mathbf{h}$  and internal rf field due to the precessing magnetization,

$$\mathbf{h}_{\text{ac}} = \mathbf{h} + \nabla_{\mathbf{M}}\mathbf{H}_K|_{\mathbf{M}_0} \cdot \mathbf{m}. \quad (28)$$

Obviously, the solution of Eq. (26) is

$$\mathbf{m} = \begin{pmatrix} \chi_L & -i\chi_T & 0 \\ i\chi_T & \chi_L & 0 \\ 0 & 0 & 0 \end{pmatrix} \mathbf{h}_{\text{ac}} = \overleftrightarrow{\chi}_{\text{P}} \cdot \mathbf{h}_{\text{ac}}, \quad (29)$$

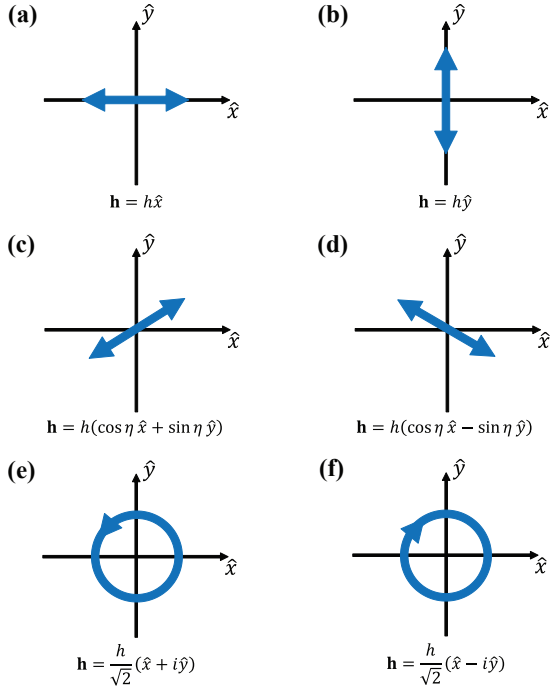


FIG. 1. Different polarizations of the applied microwave magnetic field  $\mathbf{h}$ .  $\mathbf{h}$  is linearly polarized in (a)-(d) and circularly polarized in (e) and (f). The  $z$ -axis is along  $\mathbf{M}_0$  and  $0 < \eta < \pi/2$  (in (c) and (d)).

where

$$\chi_L = \frac{\omega_r \omega_M}{\omega_r^2 - \omega^2}, \chi_T = \frac{\omega \omega_M}{\omega_r^2 - \omega^2} \quad (30)$$

with  $\omega_M = \gamma M$  and  $\omega_r = \gamma H_{dc} - i\alpha\omega$ .  $\vec{\chi}_P$  is the so-called Polder tensor<sup>4</sup> and is often assumed to be the dynamic magnetic susceptibility in analyses. The Polder tensor  $\vec{\chi}_P$  is the linear response coefficient of the magnetization to the effective ac-field  $\mathbf{m} = \vec{\chi}_P \mathbf{h}_{ac}$ . Different from  $\vec{\chi}$  which is the linear response coefficient of  $\mathbf{m}$  to the applied rf field  $\mathbf{m} = \vec{\chi} \mathbf{h}$  and measurable,  $\vec{\chi}_P$  is *not measurable because*  $\mathbf{h}_{ac}$  contains both the applied rf field  $\mathbf{h}$  and an oscillating anisotropy field due to the precessing magnetization. Obviously  $\mathbf{h}_{ac}$  *cannot be measured directly*. If one defines matrix  $\vec{W}$  as  $\vec{W} \equiv (1 + \vec{\chi}_P \cdot \frac{\delta^2 \varepsilon}{\mu_0 \delta M \delta M} |_{\mathbf{M}_0})^{-1}$ , then  $\vec{\chi}$  relates to  $\vec{\chi}_P$  as  $\vec{\chi} = \vec{W} \cdot \vec{\chi}_P$ .  $\vec{\chi}_P$  is simple and can be fully determined by a few constants even though it is not a true measurable quantity while  $\vec{\chi}$  is much more complicated and is sensitive to the magnetic anisotropy. This may be the reason why  $\vec{\chi}_P$  was so often taken as the dynamic magnetic susceptibility matrix although the real one is  $\vec{\chi}$ .

It should be interesting to know when  $\vec{\chi}$  is a Polder tensor, i.e.  $\chi_{xy} = -\chi_{yx}$  and  $\chi_{xx} = \chi_{yy}$  or  $C_2 = 0$  and  $C_1 = C_4$ , according to Eq. (18). Let us first understand the physical meanings of  $C_1 \sim C_4$ . Consider six different  $\mathbf{h}$  of amplitude  $h$  shown in Fig. 1: along the  $x$ -direction  $\mathbf{h} = h\hat{x}$  (a); the  $y$ -direction  $\mathbf{h} = h\hat{y}$  (b); the direction  $\eta$  angle with  $x$ -axis  $\mathbf{h} =$

$h(\cos \eta \hat{x} + \sin \eta \hat{y})$  (c); the direction  $\pi - \eta$  angle with the  $x$ -axis  $\mathbf{h} = h(\cos \eta \hat{x} - \sin \eta \hat{y})$  (d); the right-hand circularly polarized field  $\mathbf{h} = \frac{h}{\sqrt{2}}(\hat{x} + i\hat{y})$  (e); the left-hand circularly polarized field  $\mathbf{h} = \frac{h}{\sqrt{2}}(\hat{x} - i\hat{y})$  (f). If one denotes the microwave absorption intensities around FMR in Figs. 1(a)~1(f) by  $I_a \sim I_f$ , from Eqs. (12), (15) and (16), one has  $I_a = (0.25h^2\mu_0\omega\pi\Gamma)C_1L(\omega, \omega_0, \Gamma)$  and  $I_b = (0.25h^2\mu_0\omega\pi\Gamma)C_4L(\omega, \omega_0, \Gamma)$ , proportional to  $C_1$  and  $C_4$  respectively. Similarly,  $I_c - I_d = (0.5h^2\mu_0\omega\pi\Gamma)\sin(2\eta)C_2L(\omega, \omega_0, \Gamma)$  is proportional to  $C_2$  and  $I_e - I_f = (h^2\mu_0\omega\pi\Gamma)C_3L(\omega, \omega_0, \Gamma)$  measures  $C_3$ . Obviously,  $C_1$  and  $C_4$  are always positive whereas  $C_2$  and  $C_3$  can be positive, negative or zero, depending on the experimental setup and the choice of coordinate. Thus, one has  $\chi_{xy} = -\chi_{yx}$  if  $C_2$  is zero (or  $I_c = I_d$ ), and vice versa.

The condition for  $\chi_{xy} = -\chi_{yx}$  can be obtained from the exact solution of  $\vec{\chi}$  for an arbitrary energy landscape  $\varepsilon(\mathbf{M})$ . By solving Eq. (26),  $\vec{\chi}$  is

$$\vec{\chi} = \frac{1}{|T|^2 - PQ} \begin{pmatrix} P & T & 0 \\ T^* & Q & 0 \\ 0 & 0 & 0 \end{pmatrix}, \quad (31)$$

with

$$\begin{aligned} P &= -\frac{1}{\mu_0} \frac{\partial^2 \varepsilon}{\partial M_y^2} \Big|_{\mathbf{M}_0} - \frac{H_{dc}}{M} + i\alpha \frac{\omega}{\gamma M}, \\ Q &= -\frac{1}{\mu_0} \frac{\partial^2 \varepsilon}{\partial M_x^2} \Big|_{\mathbf{M}_0} - \frac{H_{dc}}{M} + i\alpha \frac{\omega}{\gamma M}, \\ T &= \frac{1}{\mu_0} \frac{\partial^2 \varepsilon}{\partial M_x \partial M_y} \Big|_{\mathbf{M}_0} + i \frac{\omega}{\gamma M}. \end{aligned} \quad (32)$$

Thus, one can have  $\chi_{xy} = -\chi_{yx}$  only when

$$\frac{\partial^2 \varepsilon}{\partial M_x \partial M_y} \Big|_{\mathbf{M}_0} = 0. \quad (33)$$

This could happen in several cases. If the system has rotation symmetry about  $\mathbf{M}_0$  so that the energy absorption rate of a linearly polarized microwave does not depend on the direction of  $\mathbf{h}$  in the  $xy$ -plane, then one has  $C_2 \propto I_c - I_d = 0$  and  $C_1/C_4 = I_a/I_b = 1$ . Thus,  $\chi_{xy} = -\chi_{yx}$  and  $\chi_{xx} = \chi_{yy}$ , and  $\vec{\chi}$  is a Polder tensor. An obvious example for this case is an isotropic system without magnetic anisotropy so that  $\mathbf{M}_0$  is along  $\mathbf{H}$ .  $\chi_{xy} = -\chi_{yx}$  if the free energy density is symmetric about the  $yz$ - or  $xz$ -plane, i.e.  $\varepsilon(M_x, M_y, M_z) = \varepsilon(-M_x, M_y, M_z)$  or  $\varepsilon(M_x, M_y, M_z) = \varepsilon(M_x, -M_y, M_z)$ . Take derivatives with respect to  $M_x$  and  $M_y$  on both sides, one has

$$\frac{\partial^2 \varepsilon}{\partial M_x \partial M_y} \Big|_{\mathbf{M}_0} = -\frac{\partial^2 \varepsilon}{\partial M_x \partial M_y} \Big|_{\mathbf{M}_0} = 0.$$

For an arbitrary magnetic material, it is also possible to make  $\chi_{xy} = -\chi_{yx}$  by properly choosing  $x$  and  $y$  axes. To prove this statement, let  $\vec{\chi}$ , characterized

by  $C_1 \sim C_4$ , be a non-Polder tensor in the original  $xy$ -coordinate. One can choose a new  $x'y'$ -coordinate that relates to  $xy$ -coordinate by the rotation matrix (around the  $z$ -axis)

$$\overleftrightarrow{R} = \begin{pmatrix} \cos \delta & -\sin \delta & 0 \\ \sin \delta & \cos \delta & 0 \\ 0 & 0 & 1 \end{pmatrix}. \quad (34)$$

In this new coordinate, the susceptibility matrix is  $\overleftrightarrow{R}\overleftrightarrow{\chi}\overleftrightarrow{R}^T$  characterized by new  $C'_1 \sim C'_4$ .  $C'_1 \sim C'_4$  relate to  $C_1 \sim C_4$  by

$$\begin{aligned} C'_1 &= C_1 \cos^2 \delta - C_2 \sin 2\delta + C_4 \sin^2 \delta, \\ C'_2 &= \frac{C_1 - C_4}{2} \sin 2\delta + C_2 \cos 2\delta, \\ C'_3 &= C_3, \\ C'_4 &= C_1 \sin^2 \delta + C_2 \sin 2\delta + C_4 \cos^2 \delta. \end{aligned} \quad (35)$$

If one chooses  $\delta = 0.5 \arctan \frac{2C_2}{C_4 - C_1}$ ,  $C'_2 = 0$  so that off-diagonal elements are opposite to each other in the new coordinate. Interestingly,  $C_3$  does not change while  $C_1$ ,  $C_2$  and  $C_4$  depend on the coordinate change. This is not surprising because  $C_3$  relates to the microwave absorption rate difference between the right-hand and left-hand circularly polarized rf fields which rotate around  $z$ -axis so that the choice of  $x$ - and  $y$ -axes is not matter to the energy absorption, or to  $C_3$ .

Naively, one may expect that the traditional microwave absorption experiments cannot measure a complex number such as susceptibility matrix elements, because only Lorentzian lineshapes can be measured. However, the above discussions clearly show that the traditional microwave absorption experiments are capable of completely determining the dynamic magnetic susceptibility matrix.

#### D. Determination of matrix $\overleftrightarrow{\chi}$

One of the achievements in subsection II.B is that the dynamic magnetic susceptibility can be fully characterized by a few parameters. This is important because  $\overleftrightarrow{\chi}$  expressed in terms of magnetic anisotropy, like Eqs. (31) and (32), is not too useful since the exact form of the magnetic anisotropy is hard to obtain in reality if not impossible. A natural question is how to experimentally determine these parameters. From the early discussion of the meaning of  $C_1 \sim C_4$ , a recipe, which is based on traditional FMR measurements and allows a full determination of these parameters can be obtained. The idea is to apply different  $\mathbf{h}$  as shown in Fig. 1 so that one can associate  $C_1 \sim C_4$ ,  $\omega_0$  (or  $H_0$ ) and  $\Gamma$  (or  $\Gamma_1$ ) with peak-height, peak-position, and peak-width of microwave absorption spectrum. Our recipe is:

*Step I* Use usual magnetic measurement to locate the direction of  $\mathbf{M}_0$  along which the  $z$ -axis is chosen, and a  $xyz$ -Cartesian coordinate can be assigned.

*Step II* Conduct a usual FMR microwave absorption experiment by using a microwave whose rf magnetic field  $\mathbf{h}$  is along  $x$ -axis. Either frequency  $\omega$  or field  $H$  is swept so that resonance  $\omega_0$  (or  $H_0$ ), together with linewidth  $\Gamma$  (or  $\Gamma_1$ ) can be obtained from the microwave absorption curve. As discussed early (Fig. 1),  $C_1$  is given by the peak-height  $I_a$  of the microwave absorption curve as  $C_1 = 2I_a/(\mu_0 h^2 \omega_0)$ .

*Step III* Repeat Step II but use  $\mathbf{h} = h\hat{y}$ ,  $C_4$  is given by the peak-height  $I_b$  as  $C_4 = 2I_b/(\mu_0 h^2 \omega_0)$ .

*Step IV* Repeat Step II but use  $\mathbf{h} = h(\cos \eta \hat{x} + \sin \eta \hat{y})$  first to obtain the peak-height  $I_c$  of the microwave absorption curve, then use  $\mathbf{h} = h(\cos \eta \hat{x} - \sin \eta \hat{y})$  to obtain the peak-height  $I_d$ .  $C_2$  is then given by  $C_2 = (I_c - I_d)/[(\mu_0 h^2 \omega_0) \sin 2\eta]$ .

*Step V* Repeat Step II but use  $\mathbf{h} = h(\cos \eta \hat{x} + i \sin \eta \hat{y})$  first to obtain the peak-height  $I_e$  of the microwave absorption curve, then use  $\mathbf{h} = h(\cos \eta \hat{x} - i \sin \eta \hat{y})$  to obtain the peak-height  $I_f$ .  $C_3$  is then given by  $C_3 = (I_e - I_f)/(2\mu_0 h^2 \omega_0)$ .

According to Eq. (17),  $\overleftrightarrow{\chi}(\omega)$  is fully determined from the above steps. For  $\overleftrightarrow{\chi}(H)$ , one needs to determine whether  $\beta/|\beta| = -1$  or  $\beta/|\beta| = 1$ , corresponding to the increase or decreases of  $\omega_0$  with  $H$ . Step V involves the circularly-polarized microwaves that may be difficult to obtain in experiments. However, one should notice that the recipe is not unique. One may use other easily obtained microwaves to determine  $C_3$ .

#### E. The lineshape of dc-voltage

With the general form of the dynamic magnetic susceptibility matrix  $\overleftrightarrow{\chi}$ , we can compute the AMR and AHE contributions to the dc-voltage and study the symmetry of dc-voltage lineshapes. Substituting Eq. (7) into Eqs. (4) and (5),  $U_{\text{AMR}}$  and  $U_{\text{AHE}}$  in terms of  $\overleftrightarrow{\chi}$  are

$$U_{\text{AMR}} = -\frac{\Delta\rho}{2M} \text{Re}[(j_i^* h_j l_z \chi_{ij} + j_z^* h_j l_i \chi_{ij}) e^{i(\phi_1 - \phi_2)}], \quad (36)$$

$$U_{\text{AHE}} = \frac{R_1}{2} \text{Re}(\epsilon_{ijk} j_j^* h_l l_i \chi_{kl} e^{i(\phi_1 - \phi_2)}), \quad (37)$$

where subscript indices  $i, j, k$  and  $l$  can be  $x, y$  and  $z$ . Throughout this paper,  $\epsilon_{ijk}$  is the Levi-Civita symbol, and the Einstein summation convention is used. Whether a matrix element of  $\overleftrightarrow{\chi}$  is involved in dc-voltage depends on the applied microwave fields and experimental setup. Substituting Eqs. (17) and (18) into Eqs. (36) and (37), the frequency dependence of dc-voltage can be expressed in terms of Lorentzian and  $D$  functions,

$$U_{\text{AMR}}(\omega) = A_1 \frac{\pi\Gamma}{2} L(\omega, \omega_0, \Gamma) + A_2 \frac{\pi\Gamma}{2} D(\omega, \omega_0, \Gamma), \quad (38)$$

$$U_{\text{AHE}}(\omega) = A_3 \frac{\pi\Gamma}{2} L(\omega, \omega_0, \Gamma) + A_4 \frac{\pi\Gamma}{2} D(\omega, \omega_0, \Gamma), \quad (39)$$

where the relative intensities  $A_1 \sim A_4$  are

$$\begin{aligned} A_1 &= -\frac{\Delta\rho}{2M}\text{Re}[(j_i^*h_jl_zC_{ij} + j_z^*h_jl_iC_{ij})e^{i(\phi_1-\phi_2)}], \\ A_2 &= \frac{\Delta\rho}{2M}\text{Im}[(j_i^*h_jl_zC_{ij} + j_z^*h_jl_iC_{ij})e^{i(\phi_1-\phi_2)}], \\ A_3 &= \frac{R_1}{2}\text{Re}(\epsilon_{ijk}j_j^*h_l l_i C_{kl}e^{i(\phi_1-\phi_2)}), \\ A_4 &= -\frac{R_1}{2}\text{Im}(\epsilon_{ijk}j_j^*h_l l_i C_{kl}e^{i(\phi_1-\phi_2)}), \end{aligned} \quad (40)$$

where subscript indices  $i, j, k$  and  $l$  are  $x, y$  and  $z$ .  $C_{ij}$  is the element of the  $i$ 'th row and the  $j$ 'th column of matrix  $\vec{C}$  defined in Eq. (18). The way to find the field dependence of dc-voltage is similar as that for  $\vec{\chi}(H)$ .  $A_1 \sim A_4$  are functions of  $H$ , therefore, from Eqs. (38) and (39), one has

$$\begin{aligned} U_{\text{AMR}}(H) &= A_1(H)\frac{\pi\Gamma(H)}{2}L(\omega, \omega_0(H), \Gamma(H)) \\ &\quad + A_2(H)\frac{\pi\Gamma(H)}{2}D(\omega, \omega_0(H), \Gamma(H)), \end{aligned} \quad (41)$$

$$\begin{aligned} U_{\text{AHE}}(H) &= A_3(H)\frac{\pi\Gamma(H)}{2}L(\omega, \omega_0(H), \Gamma(H)) \\ &\quad + A_4(H)\frac{\pi\Gamma(H)}{2}D(\omega, \omega_0(H), \Gamma(H)). \end{aligned} \quad (42)$$

The above expressions do not mean that  $U_{\text{AMR}}(H)$  and  $U_{\text{AHE}}(H)$  are linear combinations of Lorentzian and  $D$  functions because  $A_i$ 's ( $i = 1, \dots, 4$ ) are also functions of  $H$ . However, if the approximations of Eq. (21) are applicable, i.e.

$$A_i(H) \approx A_i(H_0) \quad (i = 1, 2, 3, 4), \quad (43)$$

then  $U_{\text{AMR}}(H)$  and  $U_{\text{AHE}}(H)$  are linear combinations of the Lorentzian and  $D$  functions,

$$\begin{aligned} U_{\text{AMR}}(H) &= A_1(H_0)\frac{\pi\Gamma_1}{2}L(H, H_0, \Gamma_1) \\ &\quad - \frac{\beta}{|\beta|}A_2(H_0)\frac{\pi\Gamma_1}{2}D(H, H_0, \Gamma_1), \end{aligned} \quad (44)$$

$$\begin{aligned} U_{\text{AHE}}(H) &= A_3(H_0)\frac{\pi\Gamma_1}{2}L(H, H_0, \Gamma_1) \\ &\quad - \frac{\beta}{|\beta|}A_4(H_0)\frac{\pi\Gamma_1}{2}D(H, H_0, \Gamma_1). \end{aligned} \quad (45)$$

The symmetric dc-voltage lineshapes are from the Lorentzian terms, and antisymmetric components are determined by  $D$  terms.  $A_1 \sim A_4$  are linear combinations of  $C_1 \sim C_4$  whose coefficients depend on magnetic anisotropy and experimental setup, and their values determine the relative weights of the symmetric and antisymmetric components.

According to Eq. (40), the phase difference  $\phi_1 - \phi_2$  between rf current density and rf magnetic field is important to dc-voltage. Several groups have found experimental evidence that the phase difference relates to many

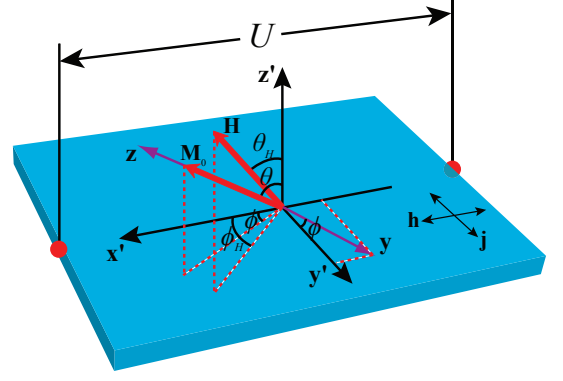


FIG. 2. Model system that mimics experimental setups in the electrical detection of FMR. The  $x'y'z'$ -coordinate is fixed with respect to the sample. The biaxial magnetic film lies in  $x'y'$ -plane. The easy axis is along  $x'$ -direction, and  $z'$ -axis is the hard axis. The  $xyz$  is a moving coordinate with the  $z$ -axis along  $\mathbf{M}_0$ , and the  $y$ -axis in the  $x'y'$ -plane.  $\theta$  and  $\phi$  are polar and azimuthal angles of  $\mathbf{M}_0$  in the  $x'y'z'$ -coordinate, i.e.  $\theta$  is the angle between the  $z$ - and  $z'$ -axes, and  $\phi$  is the angle between in-plane component of  $\mathbf{M}_0$  and the  $x'$ -axis.  $\theta_H$  and  $\phi_H$  are polar and azimuthal angles of external static field  $\mathbf{H}$  in the  $x'y'z'$ -coordinate. The directions of  $\mathbf{h}$  and  $\mathbf{j}$  are along the  $x'$ - and  $y'$ - axes, respectively.

factors like experimental setup, material parameters, microwave frequency, etc<sup>15,19</sup>. Therefore,  $\phi_1$  and  $\phi_2$  are taken as input parameters in the following discussions.

### III. VERIFICATION AND DISCUSSION

In this section, we use a biaxial model to verify the universal expressions of the dynamic magnetic susceptibility matrix and dc-voltage lineshape obtained in the last section. Both  $\vec{\chi}(\omega)$  and  $\vec{\chi}(H)$  are compared with the exact expression obtained from LLG equation (6), as well as with numerical simulations of the LLG equation.<sup>37</sup> The universal expressions of dc-voltage due to the AMR and AHE effects near FMR are compared with the exact numerical results based on the LLG equation and the generalized Ohm's law of Eq. (1).

Our model system, which mimics popular experimental setups, is shown in Fig. 2. A biaxial magnetic film lies in the  $x'y'$ -plane with length  $l$  along the  $x'$ -direction. The  $x'$ - and  $z'$ -axes are respectively the easy and hard axes of the film. For the simplicity, the rf magnetic field  $\mathbf{h}$  and the rf electric field (or rf electric current  $\mathbf{j}$ ) are along the  $x'$ - and  $y'$ -axes, respectively. A moving  $xyz$ -coordinate is defined as follows. The  $z$ -axis is along  $\mathbf{M}_0$  and the  $y$ -axis is in the  $x'y'$ -plane.  $\theta$  and  $\phi$  are polar and azimuthal angles of  $\mathbf{M}_0$  in the  $x'y'z'$ -coordinate while  $\theta_H$  and  $\phi_H$  are polar and azimuthal angles of external static field  $\mathbf{H}$  in the  $x'y'z'$ -coordinate. Therefore, once  $\mathbf{M}_0$  is determined, the  $z$ -axis is  $\hat{z} = \sin\theta \cos\phi\hat{x}' + \sin\theta \sin\phi\hat{y}' + \cos\theta\hat{z}'$ , and the  $x$ - and  $y$ -axes are determined by  $\hat{x} = \cos\theta \cos\phi\hat{x}' + \cos\theta \sin\phi\hat{y}' - \sin\theta\hat{z}'$  and



$\hat{y} = -\sin\phi\hat{x}' + \cos\phi\hat{y}'$ . The effective field of the biaxial model is

$$\mathbf{H}_{\text{eff}} = \mathbf{H} + K_1 M_{0x'}\hat{x}' - K_2 M_{0z'}\hat{z}' + \text{Re}(\mathbf{h}e^{-i(\omega t + \phi_2)}), \quad (46)$$

where  $K_1$  and  $K_2$  are respectively the dimensionless easy-axis anisotropy coefficient and hard-axis anisotropy coefficient.  $K_2$  is mainly from the shape anisotropy for a soft magnetic film so we set  $K_2 = 1$  to acknowledge this fact in this study.

According to Eq. (26), the linearized LLG Eq. in the present case becomes

$$\begin{aligned} -i\omega\mathbf{m} &= -\gamma\mathbf{m} \times (\mathbf{H} + K_1 M_{0x'}\hat{x}' - K_2 M_{0z'}\hat{z}') \\ -\gamma\mathbf{M}_0 \times (\mathbf{h} + K_1 m_{x'}\hat{x}' - K_2 m_{z'}\hat{z}') &- i\omega\frac{\alpha}{M}\mathbf{M}_0 \times \mathbf{m}. \end{aligned} \quad (47)$$

The exact solution of this equation allows us to obtain the expression of  $\vec{\chi}$ . The non-zero matrix elements of  $\vec{\chi}$  in the  $xyz$ -coordinate, according to Eq. (31), are  $\chi_{xx} = P/(|T|^2 - PQ)$ ,  $\chi_{xy} = T/(|T|^2 - PQ)$ ,  $\chi_{yx} = T^*/(|T|^2 - PQ)$  and  $\chi_{yy} = Q/(|T|^2 - PQ)$ .  $P$ ,  $Q$  and  $T$  for our biaxial model are

$$\begin{aligned} P &= K_1 \sin^2\phi - \frac{H_{\text{dc}}}{M} + i\alpha\frac{\omega}{\gamma M} \\ Q &= K_1 \cos^2\theta \cos^2\phi - K_2 \sin^2\theta - \frac{H_{\text{dc}}}{M} + i\alpha\frac{\omega}{\gamma M} \\ T &= \frac{K_1}{2} \cos\theta \sin 2\phi + i\frac{\omega}{\gamma M}, \end{aligned} \quad (48)$$

where the effective dc-field is  $\mathbf{H}_{\text{dc}} = \mathbf{H} + K_1 M_{0x'}\hat{x}' - K_2 M_{0z'}\hat{z}'$ .

In our verification of the universal expressions of Eqs. (17) and (23) below, the model parameters are chosen as  $M = 8.0 \times 10^5$  A/m and  $\alpha = 0.008$ . The value of  $K_1$  and field  $\mathbf{H}$  will vary to model different materials and experimental configurations. The phase difference  $\phi_1 - \phi_2$  between the rf current density  $\mathbf{j}$  (along  $\hat{y}'$ ) and the rf magnetic field  $\mathbf{h}$  (along  $\hat{x}'$ ) is treated as an input parameter, and the dc-voltage is measured along the  $x'$ -direction.

In Section II.B, we showed that only a few numbers are needed to fully characterize  $\vec{\chi}$ , no matter how complicated that a magnetic anisotropy of a sample might be. In order to verify this assertion, the comparison between the exact expression of  $\vec{\chi}$  and its universal form is given below for two experimental setups in which static magnetic field  $\mathbf{H}$  is applied either out of magnetic film in the  $y'z'$ -plane or in the film plane ( $x'y'$ -plane). The resultant dc-voltage lineshapes calculated from the universal form of  $\vec{\chi}$  are also compared with numerical simulations based on the LLG equation and the generalized Ohm's law.

### A. Case of $\mathbf{H}$ in the $y'z'$ -plane

In the first example, we set  $K_1 = 0.0$  ( $K_2 = 1$ ),  $\theta_H = 5.0^\circ$ ,  $\phi_H = 90^\circ$  and  $\phi_1 - \phi_2 = -90^\circ$ .  $\mathbf{M}_0$  is in

the  $y'z'$ -plane with the polar angle of  $\theta = 28.7^\circ$ , non-collinear with  $\mathbf{H}$ . Obviously, the system is symmetric about the  $y'z'$ -plane so that  $\chi_{xy} = -\chi_{yx}$ . FMR occurs at  $H = 1052.8$  mT for  $\omega = 50$  GHz. The resonance frequency  $\omega_0$  increases with  $H$ . The exact results of both real and imaginary parts of  $\chi_{xx}$ ,  $\chi_{xy}$ ,  $\chi_{yx}$  and  $\chi_{yy}$  are denoted by squares in Figs. 3(a)-3(h). Figures 3(a)-3(d) are  $\chi$ 's as functions of  $H$  at a fixed frequency  $\omega = 50$  GHz while Figs. 3(e)-3(h) as functions of  $\omega$  at a fixed field  $H = 1052.8$  mT. The black curves are the universal expressions of Eqs. (23) (for Figs. 3(a)-3(d)) and (17) (for Figs. 3(e)-3(h)) with fitting parameters of  $\Gamma = 0.87$  GHz,  $\Gamma_1 = 17.4$  mT,  $\beta/|\beta| = 1$ ,  $C_1 = 137.4$ ,  $C_2 = 0.0$ ,  $C_3 = 204.6$  and  $C_4 = 304.8$ . Curves in this example are either Lorentzian or  $D$  functions according to Eqs. (23) and (17). The perfect agreement demonstrates the validity of the universal expressions. This simple example shows that  $\mathbf{M}_0$  and  $\mathbf{H}$  are not collinear with each other even in a film made of zero-anisotropy ( $K_1 = 0$ ) magnetic materials, in contrast to the popular assumption that  $\mathbf{M}_0$  is always along  $\mathbf{H}$  for soft magnetic films such as Permalloy and Yttrium iron garnet.

The dc-voltage is computed from the LLG equation and the generalized Ohm's law. According to Eqs. (36) and (37), the dc-voltage due to the AMR involves only  $\text{Im}(\chi_{yy})$ , which is a Lorentzian function in  $H$ , while the dc-voltage due to the AHE involves only  $\text{Im}(\chi_{xy})$ , which is a  $D$  function. According to Eq. (40), the above fitting values of  $C$ 's result in  $A_1 = 73.3$  and  $A_2 = 0.0$ , in units of  $\Delta\rho jhl/M$ , and  $A_3 = 0.0$  and  $A_4 = -49.2$ , in units of  $R_1 jhl$ , where  $j$  and  $h$  are respectively the amplitudes of the rf current density and the rf magnetic field. The  $H$ -dependence of the predicted dc-voltage due to the AMR and AHE are plotted in Figs. 4(a) and 4(b) as black curves that describe perfectly the exact results (squares) from the LLG equation and the generalized Ohm's law.

To show the importance of a small non-zero magnetic anisotropy, we introduce a small  $K_1 = 0.2$  to the first example while keep all other parameters unchange. Due to the finite easy-axis anisotropy  $K_1$ ,  $\mathbf{M}_0$  is pushed out of the  $y'z'$ -plane if  $H$  is not excessive large, clearly non-collinear with  $\mathbf{H}$ . The system is not symmetric about either the  $xz$ - or  $yz$ -plane. Different from the first example,  $\chi_{xy}$  and  $\chi_{yx}$  are not opposite to each other. The exact results of both real and imaginary parts of  $\chi_{xx}$ ,  $\chi_{xy}$ ,  $\chi_{yx}$  and  $\chi_{yy}$  are denoted by triangles in Figs. 3(a)-3(h). Figures 3(a)-3(d) are  $\chi$ 's as functions of  $H$  at a fixed frequency  $\omega = 50$  GHz while Figs. 3(e)-3(h) as functions of  $\omega$  at a fixed field  $H = 875.8$  mT. Two FMR peaks appear in Figs. 3(a)-3(d) while there is only one peak in Figs. 3(e)-3(h). The direction of  $\mathbf{M}_0$  varies with  $H$  unless  $\mathbf{M}_0$  is collinear with  $\mathbf{H}$  at high values of  $H$ . As a result, the effective field also varies with  $H$ . The effective field is not a monotonic function of  $H$ . Thus,  $\omega_0(H)$  is also not a monotonic function of  $H$  as shown by the blue curve in Fig. 5. At microwave frequency  $\omega = 50$  GHz, there are two FMR peaks, or two values of  $H$  that satisfy  $\omega_0(H) = \omega$  as shown by the dashed line

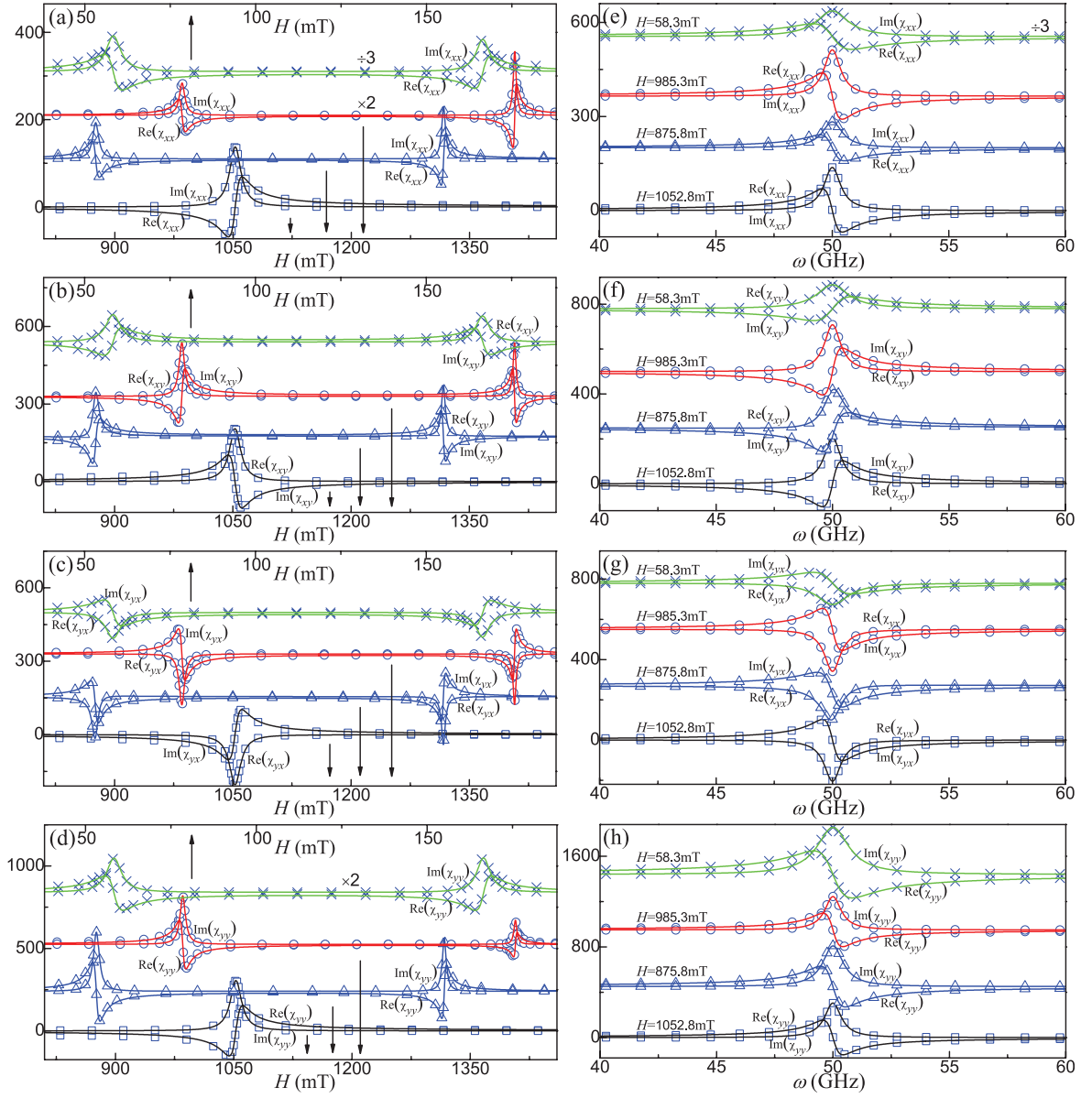


FIG. 3. The real and imaginary parts of  $\chi_{xx}$ ,  $\chi_{xy}$ ,  $\chi_{yx}$  and  $\chi_{yy}$  as functions of  $H$  at a fixed frequency  $\omega = 50$  GHz (a-d); or as functions of  $\omega$  at fixed field (e-h) with  $K_1 = 0$ ,  $K_2 = 1$ ,  $\theta_H = 5.0^\circ$  and  $\phi_H = 90.0^\circ$  (squares); or with  $K_1 = 0.2$ ,  $K_2 = 1$ ,  $\theta_H = 5.0^\circ$  and  $\phi_H = 90.0^\circ$  (triangles); or with  $K_1 = 0.2$ ,  $K_2 = 1$ , and  $\mathbf{H}$  along the  $z'$  axis (circles); or with  $K_1 = 0.1$ ,  $K_2 = 1$ ,  $\theta_H = 90.0^\circ$  and  $\phi_H = 87.0^\circ$  (cross). Symbols are the exact results from Eq. (48) and solid curves are the fittings to the universal forms of Eqs. (23) (a-d) and (17) (e-h). Curves are vertically offset (from the top down) 310, 210, 110, 0 (a); 540, 330, 175, 0 (b); 500, 330, 155, 0 (c); 840, 525, 240, 0 (d); 555, 365, 200, 0 (e); 780, 500, 250 0 (f); 780, 550, 270, 0 (g); 1440, 950, 450, 0 (h) for a better view.

of  $\omega_0(H) = 50$  GHz in Fig. 5 that cross with blue curve at  $H = 875.8$  mT, and  $H = 1317.0$  mT. For a comparison, the monotonic  $\omega_0 - H$  behavior of the first example is also plotted as the black curve in the figure. At the first peak ( $H_0 = 875.8$  mT),  $\mathbf{M}_0$  lies with  $\theta = 44.0^\circ$  and  $\phi = 33.2^\circ$ , non-collinear with  $\mathbf{H}$ . The second peak occurs at  $H_0 = 1317.0$  mT, and  $\mathbf{M}_0$  lies in the  $y'z'$ -plane with  $\theta = 18.2^\circ$ . The blue curves in Figs. 3(a)-3(h) are the universal expressions of Eqs. (23) for (a)-(d) and (17) for (e)-(h). For the curves in Figs. 3(a)-3(d), the fitting

parameters around the first (second) peak are  $\Gamma_1 = 9.2$  mT,  $\beta/|\beta| = -1$ ,  $C_1 = 83.0$ ,  $C_2 = 39.5$ ,  $C_3 = 168.1$  and  $C_4 = 359.2$  ( $\Gamma_1 = 6.0$  mT,  $\beta/|\beta| = 1$ ,  $C_1 = 118.9$ ,  $C_2 = 0.0$ ,  $C_3 = 196.1$  and  $C_4 = 323.2$ ). For the curves in Figs. 3(e)-3(h), the fitting parameters are  $\Gamma = 1.06$  GHz and the same  $C$ -values as those for the first peak in Figs. 3(a)-3(d). Different from the first example, the real and imaginary parts of  $\chi_{xy}$  and  $\chi_{yx}$  around the first peak are asymmetric functions. The perfect agreement verifies the validity of the universal expressions.

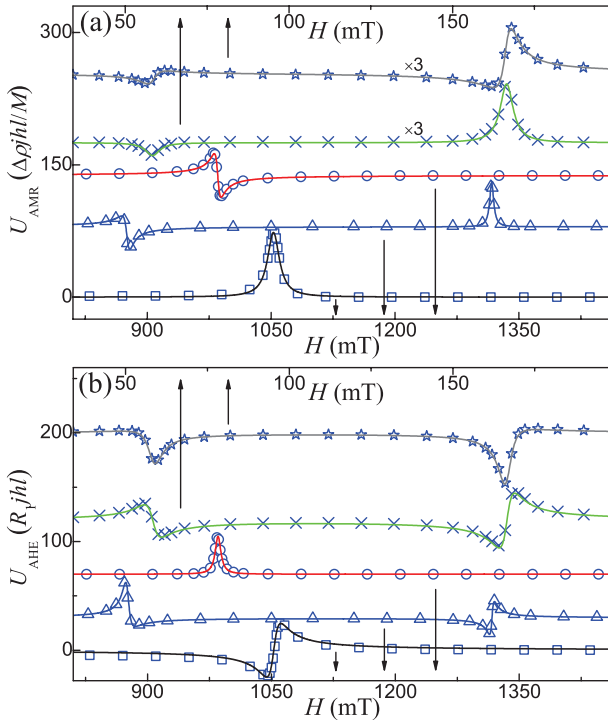


FIG. 4. The field dependence of the dc-voltage due to the AMR contribution (a) and the AHE contribution (b) at  $\omega = 50$  GHz. Model parameters are  $K_1 = 0$ ,  $K_2 = 1$ ,  $\theta_H = 5.0^\circ$ ,  $\phi_H = 90.0^\circ$  and  $\phi_1 - \phi_2 = -90^\circ$  (squares); or  $K_1 = 0.2$ ,  $K_2 = 1$ ,  $\theta_H = 5.0^\circ$ ,  $\phi_H = 90.0^\circ$  and  $\phi_1 - \phi_2 = -90^\circ$  (triangles); or  $K_1 = 0.2$ ,  $K_2 = 1$ ,  $\mathbf{H}$  along the  $z'$ -axis and  $\phi_1 - \phi_2 = -90^\circ$  (circles); or  $K_1 = 0.1$ ,  $K_2 = 1$ ,  $\theta_H = 90.0^\circ$ ,  $\phi_H = 87.0^\circ$  and  $\phi_1 - \phi_2 = -90^\circ$  (cross); or  $K_1 = 0.1$ ,  $K_2 = 1$ ,  $\theta_H = 90.0^\circ$ ,  $\phi_H = 87.0^\circ$  and  $\phi_1 - \phi_2 = -30^\circ$  (stars). Symbols are the exact results from the LLG equation and the generalized Ohm's law and solid curves are the universal expression of Eqs. (44) (a) and (45) (b) with  $A$ 's given by Eq. (40) and fitting parameters for the corresponding curves in Fig. 3. Curves are vertically offset (from the top down) 254, 175, 138, 80, 0 (a); 200, 120, 70, 30, 0 (b) for a better view.

The numerical results of the dc-voltage due to the AMR and AHE, obtained from the LLG equation and the generalized Ohm's law, are denoted by the triangles in Figs. 4(a) and 4(b), respectively. Both FMR peaks generate dc-voltage signals. According to Eq. (40) and using the fitting parameters found early for each peak,  $A$ 's are  $A_1 = -13.8$ ,  $A_2 = 35.1$  (in units of  $\Delta\rho jhl/M$ ),  $A_3 = -24.8$  and  $A_4 = -31.9$  (in units of  $R_1 jhl$ ) for the first FMR peak, and  $A_1 = 49.7$ ,  $A_2 = 0.0$  (in units of  $\Delta\rho jhl/M$ ),  $A_3 = 0.0$  and  $A_4 = -30.1$  (in units of  $R_1 jhl$ ) for the second FMR peak. The predicted dc-voltage due to the AMR and AHE (blue curves in Figs. 4(a) and 4(b)) describe perfectly the exact numerical results (triangles). For the first peak, since each of  $\mathbf{j}$ ,  $\mathbf{h}$  and  $\mathbf{l}$  is out of the  $xz$ - or  $yz$ -plane, the dc-voltage due to both the AMR and AHE depends on  $\text{Im}(\chi_{xx})$ ,  $\text{Im}(\chi_{xy})$ ,  $\text{Im}(\chi_{yx})$  and  $\text{Im}(\chi_{yy})$  according to Eqs. (36) and (37).  $\text{Im}(\chi_{xx})$  and  $\text{Im}(\chi_{yy})$  ( $\text{Im}(\chi_{xy})$  and  $\text{Im}(\chi_{yx})$ ) are asym-

metric (symmetric) about FMR peak. Consequently, the dc-voltage lineshapes due to both the AMR and AHE are asymmetric. For the second peak, since  $\mathbf{j}$  is in the  $xz$ -plane and  $\mathbf{h}$  and  $\mathbf{l}$  are along the  $y$ -axis, the dc-voltage due to the AMR relates only to  $\text{Im}(\chi_{yy})$  according to Eq. (36) and that due to the AHE relates only to  $\text{Im}(\chi_{xy})$  according to Eq. (37).  $\text{Im}(\chi_{yy})$  ( $\text{Im}(\chi_{xy})$ ) is symmetric (antisymmetric) about FMR peak. Consequently, the dc-voltage lineshapes about the second peak have the same symmetry as those in the first example.

In the third example, we set  $K_1 = 0.2$  ( $K_2 = 1$ ),  $\mathbf{H}$  along the  $z'$ -axis and  $\phi_1 - \phi_2 = -90^\circ$ .  $\mathbf{M}_0$  lies in the  $x'z'$ -plane so that the system is symmetric about the  $x'z'$ -plane (also the  $xz$ -plane). Like that in the first example,  $\chi_{xy}$  and  $\chi_{yx}$  are opposite to each other. The exact results of both real and imaginary parts of  $\chi_{xx}$ ,  $\chi_{xy}$ ,  $\chi_{yx}$  and  $\chi_{yy}$  are denoted by circles in Figs. 3(a)-3(h). The  $H$ -dependences at a fixed frequency of  $\omega = 50$  GHz are in Figs. 3(a)-3(d), and the  $\omega$ -dependences at a fixed field of  $H = 985.3$  mT are in Figs. 3(e)-3(h). Two FMR peaks appear in Figs. 3(a)-3(d) while there is only one peak in Figs. 3(e)-3(h). The two peaks are due to the non-monotonic of the effective magnetic field in  $H$ , resulting in multiple solutions (of  $H$ ) which satisfy  $\omega_0(H) = \omega$ . The non-monotonic behavior of  $\omega_0$  vs.  $H$  is shown by the red curve in Fig. 5. In the current case of  $\omega = 50$  GHz, there are two resonance fields (985.3 mT and 1407.3 mT). The first peak occurs at  $H_0 = 985.3$  mT, and  $\mathbf{M}_0$  lies in the  $x'z'$ -plane with  $\theta = 34.9^\circ$ , non-collinear with  $\mathbf{H}$ . The second peak occurs at  $H_0 = 1407.3$  mT, and  $\mathbf{M}_0$  is along the  $z'$ -axis, collinear with  $\mathbf{H}$ . The red curves in Figs. 3(a)-3(h) are the universal expressions of Eq. (23) for (a)-(d) and Eq. (17) for (e)-(h). For the curves in Figs. 3(a)-3(d), the fitting parameters around the first (second) peak are  $\Gamma_1 = 8.3$  mT,  $\beta/|\beta| = -1$ ,  $C_1 = 147.5$ ,  $C_2 = 0.0$ ,  $C_3 = 208.5$  and  $C_4 = 294.7$  ( $\Gamma_1 = 4.6$  mT,  $\beta/|\beta| = 1$ ,  $C_1 = 294.8$ ,  $C_2 = 0.0$ ,  $C_3 = 208.4$  and  $C_4 = 147.4$ ). For the curves in Figs. 3(e)-3(h), the fitting parameters are  $\Gamma = 0.85$  GHz and the same  $C$ -values as those for the first peak in Figs. 3(a)-3(d). Like the first example, each curve around FMR is either a Lorentzian or  $D$  function. The validity of the universal expressions are shown by the perfect agreement.

The exact numerical results of the dc-voltage due to the AMR and AHE are computed from the LLG equation and the generalized Ohm's law, and they are denoted by the circles in Figs. 4(a) and 4(b), respectively. Interestingly, only one peak, corresponding to the first peak in  $\chi$ 's, appears. The second FMR peak does not generate dc-voltage signals because  $\mathbf{M}_0$  is along the  $z'$ -axis and the  $x'y'z'$ -coordinate and the  $xyz$ -coordinate are coincident with each other. Thus,  $l_z = 0$ ,  $j_z = 0$  and  $\mathbf{j} \times \mathbf{m}$  is perpendicular to  $\mathbf{l}$ , and, according to Eqs. (4) and (5),  $U_{\text{AMR}} = U_{\text{AHE}} = 0$ . According to Eq. (40) and using the fitting parameters found early for the first peak,  $A$ 's are  $A_1 = 0.0$  and  $A_2 = -49.1$ , in units of  $\Delta\rho jhl/M$ , and  $A_3 = 34.8$  and  $A_4 = 0.0$ , in units of  $R_1 jhl$ . The predicted dc-voltage due to the AMR and AHE (red curves

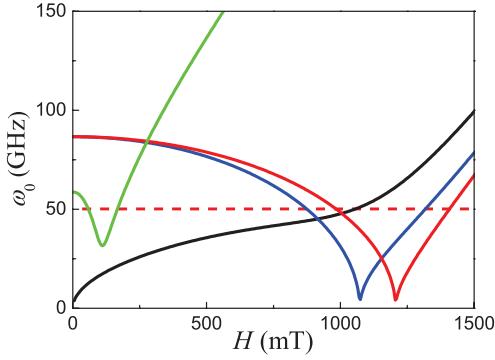


FIG. 5. The  $H$ -dependence of  $\omega_0$  for  $K_1 = 0.0$ ,  $\theta_H = 5.0^\circ$  and  $\phi_H = 90.0^\circ$  (black curves); or  $K_1 = 0.2$ ,  $\theta_H = 5.0^\circ$  and  $\phi_H = 90.0^\circ$  (blue curves); or  $K_1 = 0.2$ ,  $\mathbf{H}$  along the  $z'$ -axis (red curves); or  $K_1 = 0.1$ ,  $\theta_H = 90.0^\circ$  and  $\phi_H = 87.0^\circ$  (green curves). The dashed line is  $\omega = 50$  GHz.

in Figs. 4(a) and 4(b)) agrees again perfectly with the exact results (circles) around the first FMR peak. Since  $\mathbf{j}$  is along the  $y$ -axis and  $\mathbf{h}$  and  $\mathbf{l}$  are in the  $xz$ -plane in this case, the dc-voltage due to the AMR depends on  $\text{Im}(\chi_{yx})$  according to Eq. (36) and that due to the AHE depends only on  $\text{Im}(\chi_{xx})$  according to Eq. (37).  $\text{Im}(\chi_{yx})$  ( $\text{Im}(\chi_{xx})$ ) is antisymmetric (symmetric) about FMR peak. Consequently, the dc-voltage lineshapes have the opposite symmetry to the first example. In summary, these examples show that the dc-voltage lineshapes can change from symmetric to antisymmetric or even vanish due to magnetic anisotropy.

### B. Case of $\mathbf{H}$ in the $x'y'$ -plane

In the fourth example, we set  $K_1 = 0.1$  ( $K_2 = 1$ ),  $\theta_H = 90.0^\circ$ ,  $\phi_H = 87.0^\circ$  and  $\phi_1 - \phi_2 = -90^\circ$ .  $\mathbf{M}_0$  lies in the  $x'y'$ -plane in this case so that the system is symmetric about the  $x'y'$ -plane (also the  $yz$ -plane). With this symmetry,  $\chi_{xy}$  and  $\chi_{yx}$  are opposite to each other. The exact results of both real and imaginary parts of  $\chi_{xx}$ ,  $\chi_{xy}$ ,  $\chi_{yx}$  and  $\chi_{yy}$  are denoted by cross in Figs. 3(a)-3(h) in which Fig. 3(a)-3(d) (3(e)-3(h)) are  $H$ -dependence ( $\omega$ -dependence) at a fixed frequency of  $\omega = 50$  GHz (field of  $H = 58.3$  mT). Two FMR peaks appear in Figs. 3(a)-3(d) while there is only one peak in Figs. 3(e)-3(h). For the same reason as that for the second example, the two peaks are due to the non-monotonic of the effective magnetic field in  $H$ , resulting in multiple solutions (of  $H$ ) which satisfy  $\omega_0(H) = \omega$ . The non-monotonic behavior of  $\omega_0$  vs.  $H$  is shown by the green curve in Fig. 5. The first peak occurs at  $H_0 = 58.3$  mT, and the corresponding  $\mathbf{M}_0$  lies in the  $x'y'$ -plane with  $\phi = 33.9^\circ$ , non-collinear with  $\mathbf{H}$ . The second peak occurs at  $H_0 = 166.5$  mT at which  $\mathbf{M}_0$  lies in the  $x'y'$ -plane with  $\phi = 82.5^\circ$ , also non-collinear with  $\mathbf{H}$ . The green curves in Figs. 3(a)-3(h) are the universal expressions of Eq. (23) for (a)-(d) and Eq. (17) for (e)-(h). For the curves in Figs.

3(a)-3(d), the fitting parameters around the first (second) peak are  $\Gamma_1 = 5.2$  mT,  $\beta/|\beta| = -1$ ,  $C_1 = 27.2$ ,  $C_2 = 0.0$ ,  $C_3 = 106.3$  and  $C_4 = 415.0$  ( $\Gamma_1 = 4.8$  mT,  $\beta/|\beta| = 1$ ,  $C_1 = 24.5$ ,  $C_2 = 0.0$ ,  $C_3 = 101.2$  and  $C_4 = 417.7$ ). For the curves in Figs. 3(e)-3(h), the fitting parameters are  $\Gamma = 1.66$  GHz and the same  $C$ -values as those for the first peak in Figs. 3(a)-3(d). Similar to that of the first example, each curve around FMR is either a Lorentzian or  $D$  function. The perfect agreement verifies the validity of the universal expressions.

The exact numerical results of the dc-voltage due to the AMR and AHE, obtained from the LLG equation and the generalized Ohm's law, are denoted by the cross in Figs. 4(a) and 4(b), respectively. Both FMR peaks generate dc-voltage signals in this case. According to Eq. (40) and using the fitting parameters found early for the first (second) peak,  $A$ 's are  $A_1 = -43.5$  and  $A_2 = 0.0$ , in units of  $\Delta\rho jhl/M$ , and  $A_3 = 0.0$  and  $A_4 = -29.7$ , in units of  $R_1 jhl$  ( $A_1 = 200.1$  and  $A_2 = 0.0$ , in units of  $\Delta\rho jhl/M$ , and  $A_3 = 0.0$  and  $A_4 = -50.2$ , in units of  $R_1 jhl$ ). The predicted dc-voltage due to the AMR and AHE (green curves in Figs. 4(a) and 4(b)) describes perfectly the exact results (cross). Since  $\mathbf{j}$ ,  $\mathbf{h}$  and  $\mathbf{l}$  are all in the  $yz$ -plane, the dc-voltage around each FMR peak due to the AMR relates only to  $\text{Im}(\chi_{yy})$  according to Eq. (36) and that due to the AHE relates only to  $\text{Im}(\chi_{xy})$  according to Eq. (37).  $\text{Im}(\chi_{yy})$  ( $\text{Im}(\chi_{xy})$ ) is symmetric (antisymmetric) about FMR peak. Therefore, the dc-voltage lineshapes in this configuration have the same symmetries of  $\text{Im}(\chi_{yy})$  and  $\text{Im}(\chi_{xy})$ .

To show the importance of the phase difference  $\phi_1 - \phi_2$  between rf current density and rf magnetic field, we change this phase difference in the fourth example to  $\phi_1 - \phi_2 = -30^\circ$  while keep all other parameters in the fourth example unchanged. Obviously, the dynamic magnetic susceptibility matrix  $\hat{\chi}$  will not change. However, the symmetry of dc-voltage lineshapes change due to a different  $\phi_1 - \phi_2$ . The exact numerical results of the dc-voltage due to the AMR and AHE are denoted by the stars in Figs. 4(a) and 4(b), respectively. Similar to the previous example, both FMR peaks generate dc-voltage signals in this case. According to Eq. (40) and using the fitting parameters found early for the first (second) peak,  $A$ 's are  $A_1 = -21.7$  and  $A_2 = 37.7$ , in units of  $\Delta\rho jhl/M$ , and  $A_3 = -25.7$  and  $A_4 = -14.9$ , in units of  $R_1 jhl$  ( $A_1 = 100.1$  and  $A_2 = -173.3$ , in units of  $\Delta\rho jhl/M$ , and  $A_3 = -43.4$  and  $A_4 = -25.1$ , in units of  $R_1 jhl$ ). The predicted dc-voltage due to the AMR and AHE (gray curves in Figs. 4(a) and 4(b)) describes perfectly the exact results (stars). Since  $\mathbf{j}$ ,  $\mathbf{h}$  and  $\mathbf{l}$  are all in the  $yz$ -plane and  $\phi_1 - \phi_2 = -30^\circ$ , the dc-voltage around each FMR peak due to the AMR relates to both  $\text{Re}(\chi_{yy})$  and  $\text{Im}(\chi_{yy})$  according to Eq. (36) and that due to the AHE relates to both  $\text{Re}(\chi_{xy})$  and  $\text{Im}(\chi_{xy})$  according to Eq. (37).  $\text{Re}(\chi_{xy})$  and  $\text{Im}(\chi_{yy})$  ( $\text{Re}(\chi_{yy})$  and  $\text{Im}(\chi_{xy})$ ) are symmetric (antisymmetric) about FMR peak. Therefore, the dc-voltage lineshapes in this configuration are asymmetric.

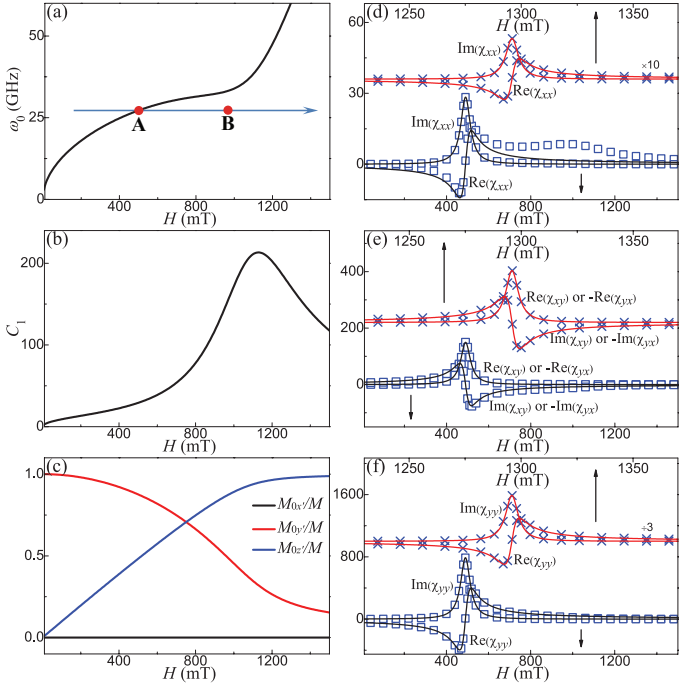


FIG. 6. The model parameters are  $K_1 = 0.0$  ( $K_2 = 1$ ),  $\theta_H = 3.0^\circ$  and  $\phi_H = 90.0^\circ$ . (a)  $H$ -dependence of  $\omega_0$ .  $\omega_0$  does not change much in the range of 400 mT  $< H < 900$  mT. At  $\omega = 27$  GHz (blue arrow line),  $\beta = 0.02$  GHz/mT. Point A and Point B are respectively the resonance and non-resonance peaks of  $\text{Re}(\chi_{xx}(H))$ . (b)  $H$ -dependence of  $C_1(H)$ . (c)  $H$ -dependence of  $M_{0x'}/M$ ,  $M_{0y'}/M$  and  $M_{0z'}/M$ . (d)-(f) The real and imaginary parts of  $\chi_{xx}$ ,  $\chi_{xy}$  (or  $-\chi_{yx}$ ) and  $\chi_{yy}$  as functions of  $H$ . Exact results are denoted by symbols, squares for  $\omega = 27$  GHz and cross for  $\omega = 60$  GHz. Solid curves are universal expression of Eq. (23) with the best fitting parameters, black for  $\omega = 27$  GHz and red for  $\omega = 60$  GHz. Top curves are vertically offset 36 (d), 220 (e) and 1000 (f) for a better view.

### C. Non-resonance peaks

So far, we have demonstrated the validity of universal expressions of Eqs. (23) and (17) for  $\hat{\chi}$ , and Eqs. (36) and (37) for dc-voltage near FMR in a number of examples as long as the approximation of Eq. (21) is good. When Eq. (21) is not good, some of the matrix elements of  $\hat{\chi}$  do not follow Eq. (23), and an extra non-resonance broad peak can even appear in some of the matrix elements near a true FMR peak in such a circumstance. To see a clear example, we set  $K_1 = 0.0$  ( $K_2 = 1$ ),  $\theta_H = 3.0^\circ$ ,  $\phi_H = 90.0^\circ$  and  $\omega = 27$  GHz.  $\mathbf{M}_0$  lies in the  $y'z'$ -plane, and the system is symmetric about the  $y'z'$ -plane (also the  $xz$ -plane) so that  $\chi_{xy}$  and  $\chi_{yx}$  are opposite to each other. Figure 6(a) shows how FMR resonance frequency  $\omega_0$  changes with  $H$ . Around relative low frequencies ( $\simeq 27$  GHz),  $\omega_0$  is not very sensitive to  $H$  with a very small  $\beta = 0.02$  GHz/mT. For both Lorentzian function  $L$  and the corresponding  $D$  function which decay as a power-law, the resonance region should

be several peak widths whose value is  $\Gamma \simeq 1$  GHz in current example. This means that the field in the resonance region can vary from about 300 mT ( $\omega_0 \sim 23$  GHz) to 1000 mT ( $\omega_0 \sim 31$  GHz). In this field range,  $C_1$  increases by more than ten times as shown in Fig. 6(b), and the direction of  $\mathbf{M}_0$ , around the  $y'$ -axis at 300 mT, moves to near the  $z'$ -axis at 1000 mT (Fig. 6(c)). Thus, one should not expect our  $\hat{\chi}$  expression of Eq. (23) good any more.

The exact results of both real and imaginary parts of  $\chi_{xx}$ ,  $\chi_{xy}$  ( $= -\chi_{yx}$ ) and  $\chi_{yy}$  as functions of  $H$  at fixed frequency  $\omega = 27$  GHz (corresponding to point A in Fig. 6(a)) are plotted as squares in Figs. 6(d)-6(f). The FMR peak occurs at  $H_0 = 490.4$  mT, and  $\mathbf{M}_0$  lies in the  $y'z'$ -plane with  $\theta = 61.8^\circ$ , non-collinear with  $\mathbf{H}$ . The black curves in Figs. 6(d)-6(f) are the universal expression of Eq. (23) with the fitting parameters of  $\Gamma_1 = 54.9$  mT,  $\beta/|\beta| = 1$ ,  $C_1 = 28.4$ ,  $C_2 = 0.0$ ,  $C_3 = 149.8$  and  $C_4 = 790.5$ . The deviation between the exact results and best fit to Eq. (23) at higher  $H$  ( $> H_0$ ) is obvious, especially for  $\text{Re}(\chi_{xx})$  whose exact result has an extra non-resonance broad peak at 970 mT.

For a comparison, we also plot the  $\chi$ 's for  $\omega = 60$  GHz at which  $\beta$  is larger and the approximation of Eq. (21) is good. The exact results of both real and imaginary parts of  $\chi_{xx}$ ,  $\chi_{xy}$  (or  $-\chi_{yx}$ ) and  $\chi_{yy}$  as functions of  $H$  are denoted by cross in Figs. 6(d)-6(f). The FMR peak occurs at  $H_0 = 1295.9$  mT, and  $\mathbf{M}_0$  lies in the  $y'z'$ -plane with  $\theta = 12.3^\circ$ , non-collinear with  $\mathbf{H}$ . The red curves in Figs. 6(d)-6(f) are the universal expression of Eq. (23) with the fitting parameters of  $\Gamma_1 = 6.8$  mT,  $\beta/|\beta| = 1$ ,  $C_1 = 172.0$ ,  $C_2 = 0.0$ ,  $C_3 = 183.8$  and  $C_4 = 196.5$ . Different from the low frequency case, Eq. (23) describes well the exact results again.

## IV. CONCLUSIONS

In this work, we show that both the dynamic magnetic susceptibility and the dc-voltage lineshapes in the electrical detection of FMR takes universal expressions near FMR for an arbitrary magnetic anisotropy. The magnetic anisotropy can affect values of those parameters that uniquely define the universal functions, but it cannot change the forms. Our explicit examples show that both the real and imaginary parts of  $\chi_{xy}$  and  $\chi_{yx}$  can be asymmetric, symmetric and antisymmetric, depending on the magnetic anisotropy and experimental setup. It is already known that interfacial interaction can change the magnetic anisotropy<sup>26-28</sup> in multilayer structures. Thus the dc-voltage signal, including its shape and symmetry, can be very different for a multilayer film and for a single magnetic layer.

In conclusion, the universal form of the dynamic magnetic susceptibility matrix is found by using the causality principle and the assumption that the frequency dependence of a usual microwave absorption lineshape around a FMR is Lorentzian. The dynamic magnetic susceptibil-

ity is not, in general, the Polder tensor that is normally assumed in the literature. The non-Polder tensor of the dynamic magnetic susceptibility has important effects on the dc-voltage lineshape in the electrical detection of a FMR. It is also found that the linear response coefficient of the magnetization to the total local rf field (sum of the applied external rf field and the internal rf field due to the precessing magnetization, a quantity cannot be measured directly) is a Polder tensor. This finding may explain why the Polder tensor was so widely misused in analyses. Although the dynamic magnetic susceptibility and dc-voltage near the FMR should depend on, in principle, the magnetic anisotropy, we show that they are fully determined by a few parameters instead of a function. These parameters can be experimentally determined by traditional microwave absorption experiments. Our results provide a reliable way to extract the dc-voltage induced by spin pumping and the ISHE. Furthermore, the non-monotonic behavior of the total effective magnetic

field in external field may lead to multiple FMR peaks in field at a constant microwave frequency while there is only a single frequency peak at a fixed static field. We also point out that insensitivity of resonance frequency to the magnetic field may lead to another broad peak which does not correspond to FMR. It raises an alarm on proper interpretation of detected FMR field peaks, especially those with broad peak and unfitable to our universal expressions.

## V. ACKNOWLEDGEMENTS

This work was supported by Hong Kong RGC grants (163011151 and 605413), grant from National Natural Science Foundation of China (11374249) and UESTC. SSK acknowledge the support of 111 Project grant (B13029).

- 
- \* [Corresponding author:]phxwan@ust.hk
- <sup>1</sup> C. Kittel, Phys. Rev. **73**, 155 (1948).
  - <sup>2</sup> H. Suhl, Phys. Rev. **97**, 555 (1955).
  - <sup>3</sup> P. E. Tannenwald, Phys. Rev. **100**, 1713 (1955).
  - <sup>4</sup> H. Seidel and H. Boyet, J. Appl. Phys. **28**, 452 (1957).
  - <sup>5</sup> Benjamin Lax and Kenneth J. Button, *Microwave ferrites and Ferrimagnetics* (New York, McGraw-Hill, 1962).
  - <sup>6</sup> M. Farle, Rep. Prog. Phys. **61**, 755 (1998).
  - <sup>7</sup> S. Mizukami, Y. Ando, and T. Miyazaki, Phys. Rev. B **66**, 104413 (2002).
  - <sup>8</sup> Y. Sun, H. Chang, M. Kabatek, Y.-Y. Song, Z. Wang, M. Jantz, W. Schneider, M. Wu, E. Montoya, B. Kardasz, B. Heinrich, S. G.E. te Velthuis, H. Schultheiss and A. Hoffmann, Phys. Rev. Lett. **111**, 106601 (2013).
  - <sup>9</sup> H. J. Juretschke, J. Appl. Phys. **31**, 1401 (1960).
  - <sup>10</sup> W. G. Egan and H. J. Juretschke, J. Appl. Phys. **34**, 1477 (1963).
  - <sup>11</sup> E. Saitoh, M. Ueda, H. Miyajima and G. Tatara, Appl. Phys. Lett. **88**, 182509 (2006).
  - <sup>12</sup> M. V. Costache, M. Sladkov, S. M. Watts, C. H. van der Wal, and B. J. van Wees, Phys. Rev. Lett. **97**, 216603 (2006).
  - <sup>13</sup> O. Mosendz, J. E. Pearson, F.Y. Fradin, G. E.W. Bauer, S. D. Bader and A. Hoffmann, Phys. Rev. Lett. **104**, 046601 (2010).
  - <sup>14</sup> L. Liu, T. Moriyama, D. C. Ralph, and R. A. Buhrman, Phys. Rev. Lett. **106**, 036601 (2011).
  - <sup>15</sup> A. Azevedo, L. H. Vilela-Leão, R. L. Rodríguez-Suárez, A. F. Lacerda Santos and S. M. Rezende, Phys. Rev. B **83**, 144402 (2011).
  - <sup>16</sup> Z. Feng, J. Hu, L. Sun, B. You, D. Wu, J. Du, W. Zhang, A. Hu, Y. Yang, D. M. Tang, B. S. Zhang, and H. F. Ding, Phys. Rev. B **85**, 214423 (2012).
  - <sup>17</sup> L. Chen, S. Ikeda, F. Matsukura, and H. Ohno, Appl. Phys. Express **7**, 013002 (2014).
  - <sup>18</sup> Y. S. Gui, N. Mecking, X. Zhou, Gwyn Williams, and C.-M. Hu, Phys. Rev. Lett. **98**, 107602 (2007).
  - <sup>19</sup> M. Harder, Z. X. Cao, Y. S. Gui, X. L. Fan, and C.-M. Hu, Phys. Rev. B **84**, 054423 (2011).
  - <sup>20</sup> A. A. Tulapurkar, Y. Suzuki, A. Fukushima, H. Kubota, H. Maehara, K. Tsunekawa, D. D. Djayaprawira, N. Watanabe, and S. Yuasa, Nature (London) **438**, 339 (2005).
  - <sup>21</sup> J. C. Sankey, P. M. Braganca, A. G. F. Garcia, I. N. Krivorotov, R. A. Buhrman, and D. C. Ralph, Phys. Rev. Lett. **96**, 227601 (2006).
  - <sup>22</sup> S. T. B. Goennenwein, S. W. Schink, A. Brandlmaier, A. Boger, M. Opel, R. Gross, R. S. Keizer, T. M. Klapwijk, A. Gupta, H. Huebl, C. Bihler and M. S. Brandt, Appl. Phys. Lett. **90**, 162507 (2007).
  - <sup>23</sup> A. Yamaguchi, H. Miyajima, T. Ono, Y. Suzuki, S. Yuasa, A. Tulapurkar, and Y. Nakatani, Appl. Phys. Lett. **90**, 182507 (2007).
  - <sup>24</sup> Y. Tserkovnyak, A. Brataas and G. E.W. Bauer, Phys. Rev. Lett. **88**, 117601 (2002).
  - <sup>25</sup> Y. Kajiwara, K. Harii, S. Takahashi, J. Ohe, K. Uchida, M. Mizuguchi, H. Umezawa, H. Kawai, K. Ando, K. Takanashi, S. Maekawa and E. Saitoh, Nature **464**, 262-267 (2010).
  - <sup>26</sup> M. Sakurai, Phys. Rev. B **50**, 3761 (1994).
  - <sup>27</sup> M. Tsujikawa and T. Oda, Phys. Rev. Lett. **102**, 247203 (2009).
  - <sup>28</sup> Z. Li, H. Xie, X. Liu, J. Bai, F. Wei, D. Wei, S. Yoshimura, H. Saito and X. Liu, J. Appl. Phys. **109**, 07D343 (2011).
  - <sup>29</sup> J. Lu and X. R. Wang, Appl. Phys. Lett. **90**, 052109 (2007).
  - <sup>30</sup> Y. Zhang, H. W. Zhang and X. R. Wang, arXiv:1510.01217.
  - <sup>31</sup> Emerson M. Pugh and Norman Rostoker, Rev. Mod. Phys. **25**, 151 (1953).
  - <sup>32</sup> T. L. Gilbert, IEEE Trans. Magn. **40**, 3443 (2004).
  - <sup>33</sup> B. Hu and X. R. Wang, Phys. Rev. Lett. **111**, 027205 (2013); X. S. Wang, P. Yan, Y. H. Shen, G. E.W. Bauer, and X. R. Wang, Phys. Rev. Lett. **109**, 167209 (2012).
  - <sup>34</sup> Z.Z. Sun and X.R. Wang, Phys. Rev. Lett. **97**, 077205 (2006); X.R. Wang and Z.Z. Sun, *ibid* **98**, 077201 (2007).
  - <sup>35</sup> Z. Z. Sun and X. R. Wang, Phys. Rev. B **74**, 132401 (2006).
  - <sup>36</sup> John S. Toll, Phys. Rev. **104**, 1760 (1956)

- <sup>37</sup> M. d'Aquino, C. Serpico, G. Miano, I. D. Mayergoyz and G. Bertotti, *J. Appl. Phys.* **97**, 10E319 (2005).